UNIVERSITAT POLITÈCNICA DE CATALUNYA
BARCELONATECH
Escola d'Enginyeria de Barcelona Est

TRABAJO FIN DE MÁSTER

Máster en Ingeniería Química

HIGH TEMPERATURE THERMOPLASTIC BASED ON POLYBENZIMIDAZOLE AND SILICA NANOCOMPOSITES

Memoria y Anexos

Autora: Laura Crespo Bartolomé
Directora: Dr. Elaine Armelin Diggroc

Convocatòria: Junio 2018

Resum

D'entre els polímers termoplàstics, el polibenzimidazol (PBI), abreviatura de poli [2,2'-(*m*-fenileno)-5,5'-bisbenzimidazol], és conegut per la seva estabilitat tèrmica i química al estar sotmès a altes temperatures. En general, es fa servir en la fabricació d'eines protectores d'alt rendiment, com ara fibres sintètiques per equips de bombers, roba d'astronautes i soldadors i parets d'avions.

No obstant això, la aplicació més recent del polímer PBI és en forma de membrana per a cel·les de combustible de membrana d'electròlit polimèric d'altes temperatures, conegut com HT-PEMFC, per les seves sigles en anglès. Les membranes de PBI han de dopar-se amb àcids inorgànics, com ara l'àcid fosfòric (PA), per tal de millorar les seves propietats conductives de manera substancial. Però, en dopar les membranes, la seva integritat física empitjora, esdevenint un dels seus majors inconvenients per a la aplicació del PBI dopat en dispositius tipus PEMFC.

La incorporació de materials inorgànics, com ara diòxid de titani, sílice o argila, en membranes d'intercanvi de protons (PEM) millora substancialment les seves propietats mecàniques i tèrmiques, segons estudis previs; i, per tant, la capacitat de la membrana per aplicacions en piles de combustible d'alta temperatura. En el present estudi, les membranes de PBI han estat preparades per colada de dissolvent després de la incorporació de nano-partícules de polietilenimina (PEI) i sílice químicament modificades (NP Si-PEI). L'ús de PEI (Mw ≈ 800 g/mol) com a agent d'acoplament de la sílice es fa per tal de millorar les interaccions interfacials entre l'entorn orgànic i inorgànic de la matriu del polímer.

En aquest projecte es presenta una descripció detallada de la síntesi i els mètodes utilitzats per a la caracterització de les noves membranes. Els resultats demostren que les membranes PBI-Si-PEI modificades químicament presenten millors propietats que les PBI no modificades . A més, les propietats elèctriques també es veuen millorades un cop s'ha dopat la membrana amb l'àcid fosfòric.

Paral·lelament, per tal de incrementar la durabilitat i les propietats mecàniques de la membrana de PBI, s'ha realitzat un estudi breu de la incorporació d'un àcid dopant diferent al PA, l'àcid dodecilbenzè sulfònic (DBSA), i es va avaluar les seves propietats conductives. Aquest àcid dopant es, a més a més, un agent plastificant, degut a l'elevat nombre de grups metilens ($-CH_2$) a la seva estructura.

Resumen

Entre los polímeros termoplásticos, el polibenzimidazol (PBI), abreviatura del poli [2,2'-(*m*-fenileno)-5,5'-bisbenzimidazol], es conocido por su excepcional estabilidad térmica y química al ser sometido a altas temperaturas. Por lo general, se emplea para fabricar herramientas protectoras de alto rendimiento como, por ejemplo, fibras sintéticas para equipos de bomberos, trajes de astronautas y soldadores, así como en paredes de aviones. Sin embargo, la aplicación más reciente del polímero PBI es en forma de membrana para celdas de combustible de membrana de electrolito polimérico de alta temperatura, conocido como HT-PEMFC, por sus siglas en inglés. Las membranas de PBI deben doparse con ácidos inorgánicos, como el ácido fosfórico (PA), para mejorar de manera sustancial sus propiedades conductivas. Sin embargo, al dopar las membranas, su integridad mecánica empeora, representando uno de sus mayores inconvenientes para la aplicación del PBI dopado en dispositivos tipo PEMFC.

La incorporación de materiales inorgánicos, tales como dióxido de titanio, sílice o arcilla, en membranas de intercambio de protones (PEM) mejora sustancialmente sus propiedades mecánicas y térmicas, según estudios previos; y, por lo tanto, la capacidad de la membrana para aplicaciones en pilas de combustible de alta temperatura. En el presente estudio, las membranas de PBI se prepararon por colada de disolvente después de la incorporación de nanopartículas de polietilenimina (PEI) y sílice químicamente modificadas (NP Si-PEI). El uso de PEI (Mw ≈ 800 g/mol) como agente de acoplamiento de la sílice va dirigido a mejorar las interacciones interfaciales entre el entorno orgánico e inorgánico de la matriz del polímero.

En el presente proyecto se presenta una descripción detallada de la síntesis y los métodos utilizados para la caracterización de las nuevas membranas. Los resultados demuestran que las membranas PBI-Si-PEI modificadas químicamente tienen mejores propiedades que las PBI no modificadas. Además, las propiedades eléctricas también se ven mejoradas una vez se ha dopado la membrana con el ácido fosfórico.

Paralelamente, con el objetivo de incrementar la durabilidad y las propiedades mecánicas de la membrana de PBI, se ha realizado un estudio breve de la incorporación de un ácido dopante diferente del PA, el ácido dodecilbenceno sulfónico (DBSA), y se evaluaron sus propiedades conductivas. Este ácido dopante es, además, un agente plastificante, debido al elevado número de metilenos ($-CH_2$) en su estructura.

Abstract

Among thermoplastics polymers, polybenzimidazole (PBI), short for poly [2, 2'-(*m*-phenylene)-5,5'-bisbenzimidazole], is known for its exceptional thermal and chemical stability at elevated temperature. It is usually employed to fabricate high-performance protective tools such as synthetic fibers for firefighter's gear, astronaut and welder's suits, as well as in aircraft walls, as for examples. However, the most recent application of PBI polymer is as membrane in high-temperature polymer electrolyte membrane fuel cell (HT-PEMFC). PBI membranes must be doped with inorganic acids, like phosphoric acid (PA), to substantially improve their conductivity properties. Nevertheless, when doped, its mechanical integrity gets much worse, representing one of their major handicaps for the application of doped PBI in PEMFC devices.

The addition of inorganic materials, such as titanium dioxide, silica or clay, into proton exchange membranes (PEM) is known to substantially improve their mechanical and thermal properties, as reported in previous studies; and, hence the capability of the membrane for high temperature fuel cell applications. In the present study, PBI membranes were prepared by solvent casting after the incorporation of chemically modified polyethyleneimine-silica nanoparticles (Si-PEI NPs). The use of PEI (Mw ≈ 800 g/mol) as silica coupling agent is intended to improve the interfacial interactions between the organic-inorganic surrounding in the polymer matrix.

A detailed description of the synthesis and the methods used for the characterization of the new membranes is reported. Results demonstrated that chemically modified PBI-Si-PEI membranes have better properties than the pristine PBI films. Moreover, the conductive properties were also enhanced after the doping process with the PA molecules.

Additionally, to the study above mentioned, another dopant molecule composed by dodecylbenzenesulfonic acid (DBSA) was investigated. It consisted in a brief study where the conductive properties were also approached. The DBSA molecules perform as dopant and plasticizer, due to the high number of methylene groups inside its chemical structure.

Acknowledgements

First, I would like to thank my tutor, Dr. Elaine Armelin Diggroc, for giving me the opportunity to conduct this research, and for her dedication. I would also like to thank the dedication and daily support in the laboratory of Ms. Brenda Molina.

I also would like to acknowledge Mr. Amir Aiman Bin Tahrim (University of Kuala Lumpur, Malaysia) for his help with the PBI synthesis and nanoparticles characterization; as well as Dr. Lourdes Franco and Mr. Francisco José Calvo, for their help with the thermal analyses.

This work was supported by MINECO (MAT2015-69367-R) and the Agència de Gestió d'Ajuts Universitaris i de Recerca (2017SGR359).

Glossary

Al_2O_3: aluminion oxide

AMS: amine functionalized silane

APTES: 3-aminopropyltriethoxysilane

APU: auxiliary power unit

ASMs: acidic surfactant like molecules

CHP: combined heat and power

CO_2: carbon dioxide

CO: carbon oxide

DBSA: Dodecylbenzenesulfonic acid

DLS: dinamic light scattering

EIS: electrochemical impedance spectroscopy

EtOH: ethanol

FA: formic acid

FTIR: fourier-transform infrared spectroscopy

***HT-PEMFC*:** high-temperature polymer electrolyte membrane fuel cell

ILs: ionic liquids

LAMS: long chain amine functionalized modified silica

OBA: 4, 4'-oxybis (benzoic acid)

OPBI: poly (4,4'-diophenylether-5,5'-bibenzimidazole)

ORR: oxygen reduction reaction

PA: phosphoric acid

PBI: poly [2, 2'-(m-phenylene)-5, 5'-bisbenzimidazole]

PEI: polyethyleneimine

PEM: proton exchange membrane

PEMFC: proton exchange membrane fuel cell

PFSA: persulfonic acid membranes

RAMAN: RAMAN spectroscopy

SEM: scanning electron microscopy

SI: silica

SiO_2: silicon dioxide

Si-PEI NPs: polyethyleneimine-silica nanoparticles (Si-PEI NPs).

TAM: 3, 3', 4, 4'-tetraaminobiphenyl

TEM: transmission electron microscopy

TEOS: tetraethylorthosilicate

Tg: glass transition temperature

TGA: thermogravimetric analysis

TiO_2: titanium dioxide

TMSPDT: N-(3-trimethoxysilylpropyl) diethylenetriamine

UMS: unmodified silica

WCA: water contact angle

WAXD: wide angle X-ray diffraction

ZrO_2: zirconium dioxide

ZrP: zirconium phosphates

Index

1. Preface

1.1. Origins and motivations

Current state-of-the-art proton exchange membranes (PEMs) based on perfluorosulfonic acid membranes (PFSA), as in the Nafion membrane, exhibit desirable conductivity (10^{-1} S·cm^{-1} or higher) only at elevated hydration levels. This imposes the thermal constraint that fuel-cell operating temperatures remain below 100^{0}C. As a result, a variety of challenges arise, such as decreased cathode performance, challenging system design (including the necessity of cooling and humidification units), and the necessity of fuel processing due to the low tolerance of the anode catalysts towards fuel impurities such as CO. These difficulties provide a strong driving force for the development of membranes capable of operating at elevated temperatures (>100^{0}C). At higher temperatures, the sluggish kinetics of the oxygen reduction reaction (ORR) improve, and there is an increased tolerance towards fuel impurities. This means reformed fuel feedstocks could be used as opposed to purified fuels (1). These benefits would culminate in a significant decrease in both fabrication and running costs of PEMFCs. Although improvements have been made to the Nafion systems, allowing their use at elevated temperatures and lower humidity levels, (1)(2) there is still broad scope for PEM development with a view to increasing the operating temperature of PEMFCs.

One strategy to achieve high temperature operation is to use a thermally stable polymer matrix that is less dependent on humidification for high ionic conductivity. One of the more successful high-temperature polymer membrane systems developed to date is phosphoric acid-doped poly [2, 2'-(m-phenylene) - 5, 5'-bibenzimidazole] (PBI_4N). On its own, pure PBI_4N is an electrical insulator with a glass transition temperature (Tg) of roughly 430^{0}C. It has good chemical resistance and excellent thermal properties that give rise to its diverse applications ranging from textiles to blood dialysis machines. Due to the polymers inherent basicity (pKa 5,5 as protonated), it forms strong interactions with acids (usually H_3PO_4) that renders PBI_4N a proton conductor (3). The use of PBI_4N membranes in PEMFCs was first demonstrated at elevated temperatures (100–200^{0}C) under anhydrous conditions in the mid-1990s (4). This stimulated a number of studies into polybenzimidazole (PBI) systems probing areas such as synthesis and functionalization, structural and mechanical properties, water uptake, fuel crossover, thermal stability, water drag, as well as fuel diversity.

The alternative PEMs are classified into three categories: (1) modified Nafion composite membranes; (2) functionalized non-fluorinated membranes and composite membranes therein; and (3) acid-base composite membranes. The Innovation in Materials and Molecular Engineering Group (IMEM's Group) has experience working with the third category, where new sulfonated polystyrene and styrene−ethylene/butylene−styrene block copolymer films, for applications in electrodialysis, have been prepared and characterized in collaboration with the Universidade Federal do Rio Grande do Sul (UFRGS, Brazil). (5)(6)

Regarding the present study, the phosphoric acid-doped polybenzimidazole films, to be prepared and characterized, were developed in collaboration with the University of Kuala Lumpur (Malaysia). It is important to emphasize that the IMEM's Group has no previous experience on their synthesis or applications. By contrary, our Group has previous experience in silica nanoparticles functionalization and in polyethylenimine compounds with relevance in different fields. Therefore, all the results reported here will inherently provide new insights for continuous advance in this technology, as well as in the career development plan of our future chemical engineer students.

2. Introduction

A fuel cell is an electrochemical energy conversion device for the production of efficient, environmentally friendly, and economical power supplies. Proton exchange membrane fuel cells (PEMFCs) (*Figure 2.1*) are the most promising alternatives for portable power applications. PEMFC works by electrochemical reaction, which converts chemical energy of hydrogen and oxygen into electricity and heat. The reaction in the PEMFC occurs as follows:

$$Anode: H_2 \rightarrow 4H^+ + 4e^- \qquad \textbf{(Eq. 2.1)}$$

$$Cathode: O_2 + 4H^+ + 4e^- \rightarrow 2H_2O \qquad \textbf{(Eq. 2.2)}$$

$$Overall: 2H_2 + O_2 \rightarrow 2H_2O \qquad \textbf{(Eq. 2.3)}$$

Hydrogen is reduced to hydrogen ions at the anode side and travels to cathode through electrolyte membrane. This will produce electrical current and water as by-products. In the PEMFC, PEM is an important component to the PEMFC as it not only acts as an electrolyte, which allows protons to transfer from anode to cathode, but it also acts as a barrier to prevent mixing between fuel and air.

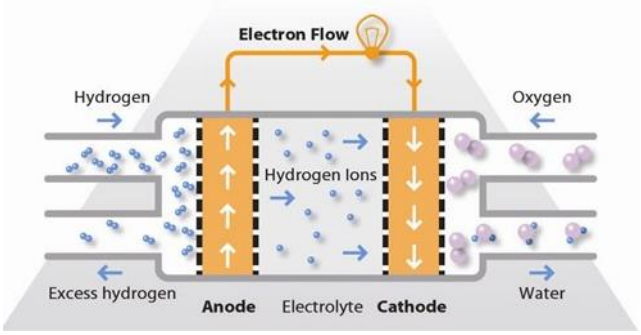

Figure 2. 1. Proton exchange membrane technology (7)

In recent years, much effort has been focused on developing new and low-cost polymer electrolyte membranes as substitutes for the very expensive sulfonated perfluoropolymers. Also, many of these efforts have been focused on how to increase the operating temperature beyond 100^0C, which is the main drawback of the Nafion membrane. Recently, phosphoric acid (PA) doped polybenzimidazole (PBI) membranes have emerged as promising candidates for low-cost and high-performance polymer electrolyte membrane materials for high-temperature polymer electrolyte membrane fuel cells operating above 120^0C.(8)

Among the variety of PEMFCs, the high temperature proton exchange membrane fuel cells (HT-PEMFCs) are proficient clean energy conversion devices for automotive and stationary applications. HT-PEMFC could mitigate the CO poisoning, humidity and heat management, and sluggish of oxygen reduction reaction (ORR). As mention above, acid doped polybenzimidazoles (PBIs)/functionalized PBIs polymer electrolyte membranes are familiar uses for HT-PEMFC because of **high proton conductivity** with **thermo-mechanical stability**. Proton conductivity of PBI membranes is greatly promising by acid doping dimension and cell operating temperature.(9)

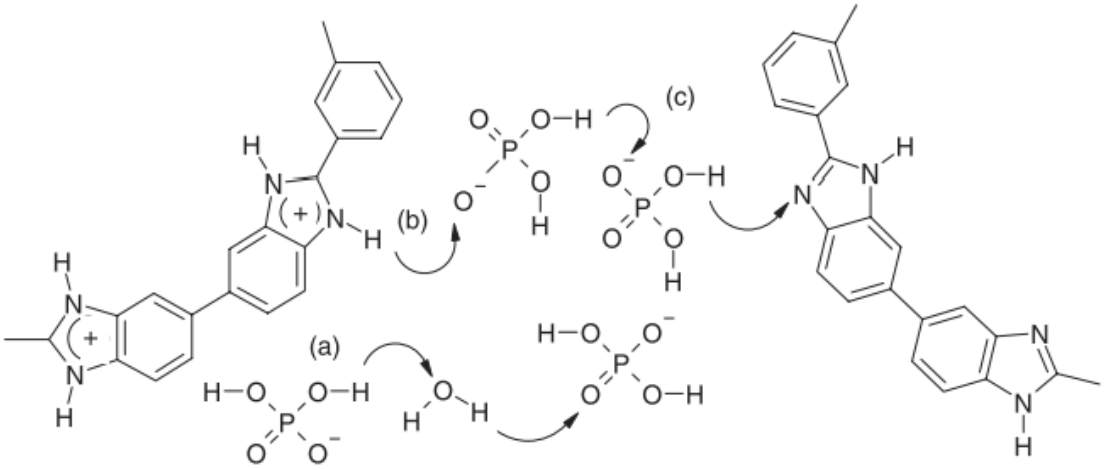

Figure 2. 2. Proton conductivity mechanism of PA-doped PBI membrane (a) PA-water proton transfer; (b) proton transfer between PA molecules; (c) benzimidazole ring-PA proton transfer (10)

PBI membrane needs to be doped with acid in order to facilitate the movement of protons across the membrane. The movement of proton in the acid doped PBI membrane are commonly through Grotthus mechanism (*Figure 2.2*). Due to the present of benzimidazole rings in the chemical structure, PBI membranes can be doped with different kind of acids. The choice of acid used affects the maximum proton conductivity properties. Savadogo & Xing (10) show that different effect of acid used to dope PBI membrane gives different level of photon conductivity. The proton conductivity changes as follow: H_2SO_4 > H_3PO_4 > $HClO_4$ >HNO_3 >HCl. Doping PBI with sulphuric acid gives the best proton conductivity however, phosphoric acid are commonly used nowadays are due to sulphuric acid doped membrane still required humidification and phosphoric acid doped membrane are able to operate under anhydrous condition (11).

Although increased number of reports in recent years on proton exchange membrane (PEM) developed from nanocomposites of polybenzimidazole (PBI) with inorganic fillers brought hope to end the saga of contradiction between proton conductivity and variety of stabilities, such as mechanical, thermal, chemical, etc.; it still remains a prime challenge to develop a highly conducting PEM with superior aforementioned stabilities. In fact, the very limited understanding of the

interactions, especially interfacial interaction between PBI and inorganic filler, leads to confusion over the choice of inorganic filler type and their surface functionalities.(12) Taking clue from T. Jana's early study (12) based on poly (4,4'-diphenylether-5,5'-bibenzimidazole) (OPBI)/silica nanocomposites, where silica nanoparticles modified with short chain amine showed interfacial interaction-dependent properties, in that work they explored the possibility of enhanced interfacial interaction and control over the interface by optimizing the chemistry of the silica surface.

2.1. High temperature thermoplastic: polybenzimidazole (PBI)

Polybenzimidazoles are a class of extremely heat-resistant heterocyclic thermoplastics. They are prepared from an aromatic tetraamine and an aromatic dicarboxylic acid or a derivative of it (*Figure 2.3*). A prominent example is the condensation reaction of diphenyl isophthalate and 3,3',4,4'-tetraaminodiphenyl which undergo spontaneous cyclization at temperatures around 350 to 400 °C in an inert atmosphere.(13)

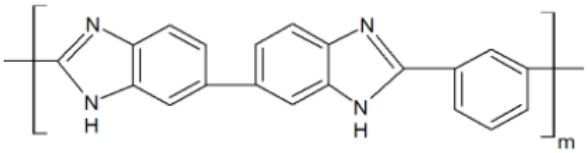

Figure 2. 3. Chemical repeating unit of PBI (13)

PBI is an amorphous thermoplastic polymer with a glass transition temperature of 425-436^{0}C and no melting point, and with heat deflection temperature at 1.8 MPa is about 435°C. It has a good chemical resistance and excellent textile fibre properties (14). Its decomposition temperature is more than 500°C (13). In form of a membrane, PBI has received much attention mainly for use in blood dialysis and reverse osmosis at high temperature and in harsh environment. (15)

Chemically, PBI is a basic polymer and can readily react with acids. As a result, various inorganic acids were investigated such as H_2SO_4, H_3PO_4, $HClO_4$, HNO_3, HBr, HCl, organic acids like CH_3SO_3H, C_2 H_5SO_3H and aromatic phosphoric acids, as well as polymeric acids. (14)

Among the doping acids, phosphoric acid and sulphuric acid were found to give high conductivity. The acids act both as donors and acceptors in proton transfer and therefore allow for proton migration along the anionic chain. H_3PO_4 is an interesting acid due to its conductivity and thermal stability at temperatures up to 200^{0}C. The PBI cells have been operated at temperatures up to 200^{0}C without humidification of the reactant gases. (9)(14)

Thus, the acid doping level is an important parameter that will affect the performance and durability of the PEMFCs. The acid doping level is defined as the mole number of phosphoric acid per repeat unit of PBI and was found to be of special importance for proton conductivities and mechanical properties (12)(14)(16).

The performance of a membrane is dependent on proton conductivity, as mention above, which in turn often depends on its water content. High proton conductivity is supported by high level of water uptake; at the same time, it is also a sign of low-dimensional stability as water influences the polymer microstructure and mechanical properties. Since water is also known to assist the mass transport of methanol and oxygen through the membrane, the water uptake measurements could serve as a quantitative measure of membrane performance for DMFC application as well. Gravimetric technique has been widely used for this purpose. Water uptake measurements are generally done by double weighing. 'Wet' weights of the membranes are first measured after equilibrating with water at different temperatures or upon exposure to water vapour at various pressures. The membrane samples are then dried at a temperature above the boiling point of water for a particular period of time and their 'dry' weight is measured. (17)

Ion exchange capacity is the measure of relative concentration of acid groups within polymer electrolyte membranes. Proton conductivity and water uptake both rely heavily on the concentration of ion conducting units in the polymer membrane. The ion content is characterized by the mass of dry membrane per molar equivalent of ion conductor. Varying the ion content of the membrane can control both its water uptake and conductivity. While it is desirable to maximize the conductivity of membrane by increasing its ion content (decreasing equivalent weight), other physical properties must be considered. Too many ionic groups will cause the membrane to swell excessively with water, which compromises mechanical integrity and durability.(17)

Other properties can be taken into account for a more detailed characterization of the PBI membranes, among them: gas and liquid permeability, durability tests, mechanical strength, etc…are some examples. However, in order not to extend too much the introduction, more detailed description of such properties and their complete characterization techniques can be access in some reviews published in the literature.(17)(18)

2.2. Applications of polybenzimidazole (PBI) membranes

Polybenzimidazoles are known for their high-strength and high-temperature performance, as explained before. They find applications in many industrial fields including semiconductor, petrochemical and aerospace industries. Major applications include heat resistant apparels, contact

seals, wafer carriers, membranes for various separation processes, insulator bushings, and thermal isolators.(13)

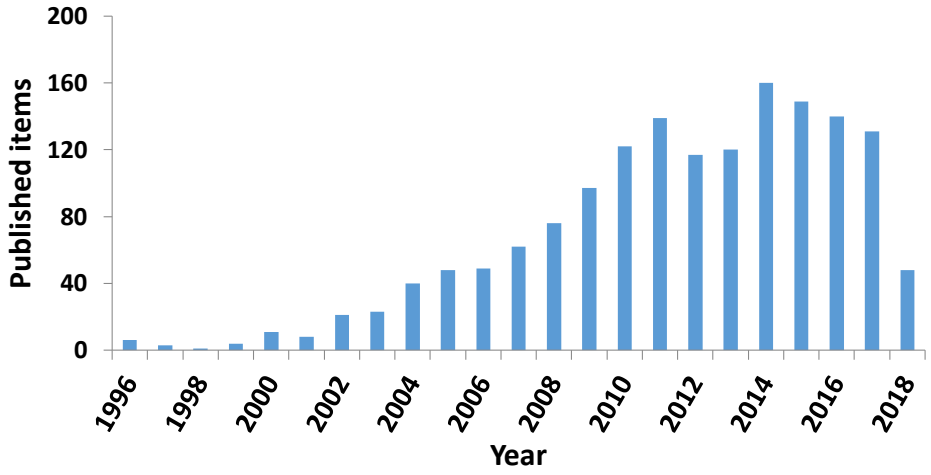

Figure 2. 4. Accumulative published items of the topic "polybenzimidazole" and "fuel cells" indexed within Web of Science (18)

One of the main applications of PBI membranes is its use in fuel cells. As seen in the *Figure 2.4*, there has been an increase on the number of publications that mention both the topic "polybenzimidazole" and "fuel cells". From a technological application point of view, PBI-based fuel cells seem most suited for stationary power applications, for example, based on the natural gas reforming and combined heat and power (CHP) generation. For automobile applications more challenges exist by considering startup time and thermal/load cycling, however, an auxiliary power unit (APU)-like system is of special interest. Volkswagen has presented at the 2007 Los Angeles Motor Show a hybrid concept car with a PBI stack as a charger for batteries to extend the driving range. As small power units, the PBI-based cells have the potential to integrate with a simplified methanol reformer or metal hydride tank (18). In addition, this proton conducting polymer electrolyte opens the door for many other electrochemical applications that could benefit from or require higher temperatures such as hydrogen gas pumping and purification (19), electrochemical sensors and water electrolysis.(18)

Subianto (11) did mention that poly(4,4-diphenyl ether-5,5-bibenzimidazole) or OPBI membrane is one of the PBI derivatives which have excellent properties to be use as membrane in HT-PEMFC. It has gained popularity nowadays (8)(12)(16). OPBI membrane has a readily tuneable molecular weight as well as relatively more flexible backbone due to presence of ether linkage (-O-) in the backbone (*Figure 2.5*) compared to other PBI structures (*Figure 2.3*) (8). Introduction of ether linkages may facilitate the entanglement between molecular chains thus forming intertwined polymer networks. The intertwined structured provide a 'sponge like' microstructure which provide "free volume" to hold excess acid molecules (20). OPBI membrane also has a better solubility in low boiling point

volatile solvents such as formic acid, employed for its synthesis. In order to improve the membrane durability and the proton conductivity, silica is added into OPBI films to obtain new composite membranes with the aid of silane coupling agents.

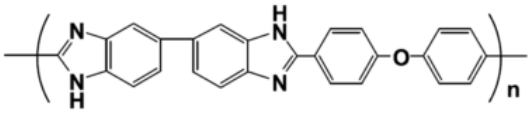

Figure 2. 5. Molecular structure of poly (4, 4'-diphenylether-5, 5'.bibenzimidazole) (OPBI)

2.3. Polybenzimidazole (PBI) composites

Various strategies have been applied to improve the stability and conductivity of PBI membranes including optimization of membrane fabrication techniques, crosslinking of polymer backbone, blending with other polymers, and forming composite structure by incorporation of various inorganic acids. However, the improvements brought by such modifications have been found rather limited and the PBI-based membranes remained demonstrating weakness in mechanical strength when highly loaded with PA and poor endurance when tested for long term.(20)(21)

In order to solve this problem, modification of the PBI matrix by addition of inorganic filler is required. Inorganic fillers are typically added to increase the proton conductivity and/or acid uptake of PBI membranes. The combine of hydrophilic inorganic nanomaterial with a PBI creates favorable results, because of their affinity to interact with the water and acid and turn out to be more hydrophilic. Most types of HT-PEMFC membranes have successfully been doped with inorganic filler such as hygroscopic oxides (SiO_2, TiO_2, ZrO_2, Al_2O_3); montmorillonite, clays, heteropolyacids and zirconium phosphates (ZrP) (22) and zeolites (17). This project focuses on the inorganic fillers and acid/plasticizer component for the obtaining of OPBI composite membranes.

Ceramic nanoscale and mesoscale fillers such as titania and zirconia have been used to design composite PA doped PBI-based membranes with appealing properties. Particularly, ZrO_2 fillers were recently tested for enhancing the conductivity and stability of PA doped PBI membranes. However, the use of nanoscale ZrO_2 filler and the accompanied membrane casting is challenged by agglomeration and precipitation leading to drastic phase inhomogeneity, despite the improvement in the hydromechanical properties by the reinforcement.(21)

Among different inorganic additives, SiO_2 is well known for its barrier property towards gases and solvents along with its strong H-bonding capability to acids, which is beneficial for the prevention of the acid leaching and improve the proton conductivity of the resulting hybrid membranes compared

to the virgin membrane (22). It is also reported that the introduction of the silica particles into the PBI matrix improved the thermal stability (22) as well as mechanical properties of the membranes that are important features for HT-PEMFC application.

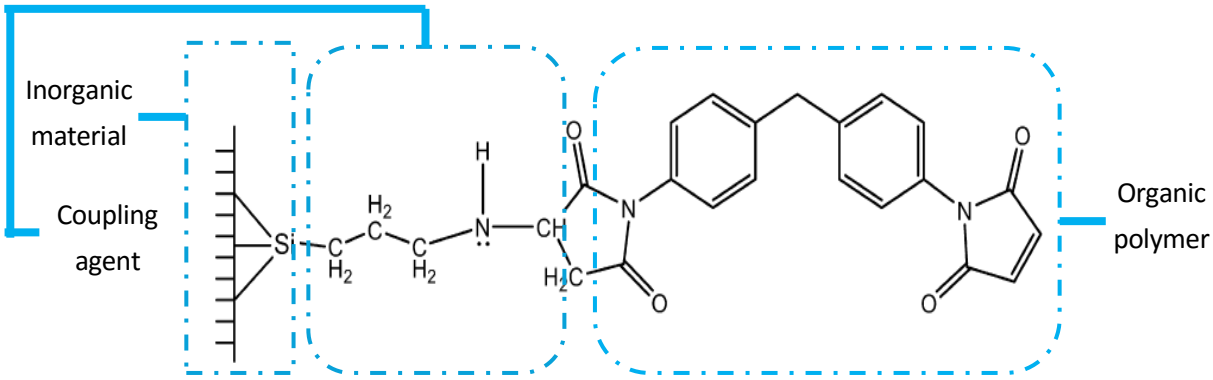

Figure 2. 6. Schematic structure: How silane coupling agent works.

The main drawback for SiO_2 filler is its insulating capability, for this reason, a low percentage of this compound is suggested to be added to the PBI matrix in order to ensure the conductivity of the membrane. Less than 2,0 wt% was used in this study.

As stated earlier, addition of SiO_2 did reduce the proton conductivity (23)(24) (reduction about 22 – 28% of conductivity compared to pure-acid doped PBI membrane). In order to overcome this problem, several studies have tried to solve this problem in the past by means of employing different kinds of amine silane coupling agents: (3-aminopropyltriethoxysilane (APTES) and N-(3-trimethoxysilylpropyl) diethylenetriamine (TMSPDT) (*Figure 2.6*) (12)(25). Most of them addressed the issue to improve the proton conductivity without compromising the mechanical stability of the membrane(25). By using amine functionalized (AMS) silane coupling agent, it was found out in the characterization of structure and evaluation of crystallinity of the composite membrane, AMS/OPBI shows several peaks in the wide angle X-ray diffraction (WAXD) patterns while unmodified silica (UMS)/OPBI doesn't show similar trend. The crystalline peaks indicate an ordered structure due to the fact that the silica particles are highly dispersed in the OPBI matrix with the help of $–NH_2$ moieties of AMS and imidazole moieties on the OPBI.

As for thermal stabilities, initial weight loss (20% loss) of composite begin at temperature 191^{o}C for 15 wt% UMS/OPBI, while for 15 wt% AMS/OPBI begin at temperature 226^{0}C and; at a temperature of 510^{0}C, 15 wt% UMS/OPBI show a residual weight loss of 69,46% and 77,99% for 15 wt% AMS/OPBI. It is suggested that a well self-assembled cluster in the nanocomposite membrane is responsible for the improvement in the thermal stabilities(25). On the hand, as for proton conductivity; 20 wt%

AMS/OPBI shows the highest proton conductivity which is 1.23 x 10^{-1} S·cm^{-1}. As for 15 wt% AMS/OPBI, it has the higher proton conductivity compared to 15 wt% UMS/OPBI which is around 1.23 x 10^{-1} S·cm^{-1} where 15 wt% UMS/OPBI has around 0.07 x 10^{-1} S·cm^{-1}. It was concluded that: morphology of OPBI/silica membrane is dependent upon the functionalized groups of silica surface, amine modified silica (AMS) helps to produce self-assembled clusters formation and unmodified silica (UMS) shows a well-dispersed formation (25). The thermal stabilities and proton conductivity are also improved with the addition of the filler.

In the study conducted by Singha et. al. (11), a long amine silica agent was used to functionalize the surface of silica nanoparticle before it was incorporated into OPBI/silica nanocomposite membrane. The long chain amine functionalized modified silica (LAMS) was used because they anticipated improved membrane properties that might arise because of the increase in the chain length and stronger multiple point interaction between three amine groups on the surface of silica and the polymer matrix. In the WAXD patters, crystalline peaks also formed but at the higher concentration (7 wt% of LAMS/OBPI and above). Compared to the previous study described, formation of self-assembled cluster is well defined as they suggested that due to the stronger interaction between three amine functionality and OPBI matrix (25). As for the thermal stabilities, it was reported that the thermal stability increased as the loading of the silica increased (at 15 wt% LAMS/OBPI shows the lesser mass loss (4% weight loss) compare to neat OBPI (7% weight loss) while 15 wt% UMS/OPBI does not show any significant improvement.).

In the proton conductivity test, which was conducted at 160^{0}C, the results showed that the conductivity for 15 wt% LAMS/OPBI was 0,181 S·cm^{-1}, while pristine OPBI was 0,118 S·cm^{-1}. However, another study, conducted by Ghosh *et al.* (26), showed that the conductivity increased as the filler loading increased because the PA doping level was also enhanced. On the other hand, other similar analysis, conducted by Singha *et al.* (12), showed a different result. *Chart 2.1* shows the comparison data between these two studies. They also suggested that the three-amine group on the silica formed hydrogen bonding with OPBI chain to produce crystallites all over the matrix. This crystal formation provides a proton-conducting channel in the matrix that helps an efficient and ease proton hopping across the membrane. They also highlighted that bare silica particles did not create proton-conducting pathways, but creates a barrier that cause tortuosity of the diffusive path for the incoming protons. In other words, the proton is forced to wiggle around the particles travelling through a tortuous path, which results in the decreasing of the proton conductivity.

Chart 2. 1. Comparison of proton conductivity (at 160^{0}C) and PA doping level (mol/RU)[a)] of AMS/OPBI and LAMS/OPBI nanocomposite membrane.

Nanofiller loading (wt%)	Proton conductivity at 160^{0}C (S·cm^{-1})		PA doping level (mol/RU)	
	AMS/OPBI composite	LAMS/OPBI composite	AMS/OPBI composite	LAMS/OPBI composite
4	0,062	0,157	21,75	26,7
7	0,073	0,159	22,75	25,3
10	0,093	0,176	24,43	24,3

Note: [a)] RU: repeat unit

By modifying the surface of silica nanoparticle with amino (-NH_2) silane agent, there were improvements in terms of better interfacial interaction and better proton conductivity compared to non-modified particle. Both studies concluded that due to the increase in the number of hydrogen bonding between the amino moieties (-NH_2) of silane agent and imidazole group of OBPI membrane which create proton conducting channels which are responsible for higher proton conductivity. Hence, it was proposed that the usage of silane coupling agent with different aliphatic amine chain (*Figure 2.7*), which has the same alkoxy group (methoxy; -OCH_3), towards the properties of composite membrane, especially for the HT-PEMFC application.

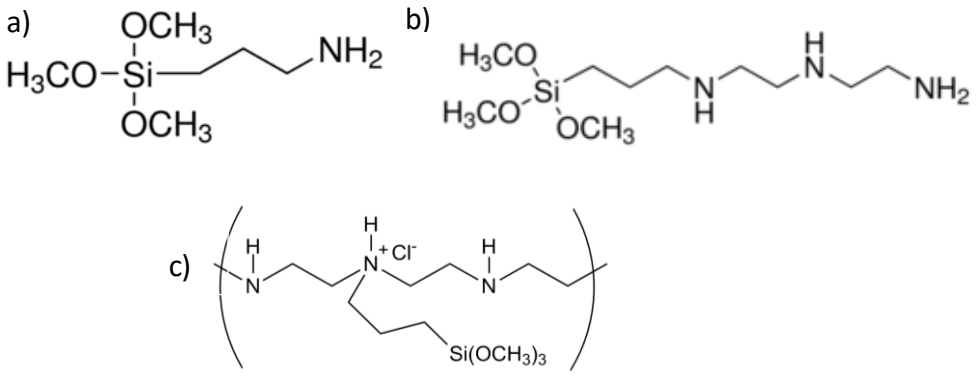

Figure 2. 7. Types of amine silane coupling agent: (a) (3-aminopropyl) trimethoxysilane (APTMS); (b) (3-trimethoxysilylpropyl) diethylenetriamine (TMSPDT); (c) trimethoxysilylpropyl modified polyethyleneimine (TMS-PEI)

2.4. Polybenzimidazole (PBI) composites with plasticizers

One of the main problems associated with polybenzimidazoles seems to be their poor solvent solubility, which results from the high degree of molecular rigidity in the backbone and the strong intra-interchain hidrogen bonding interactions, coming in the way of development of new applications (27), as well as the dehydration of phosphoric acid observed at temperatures above 180^0C, which results in serious conductivity decrease (28). Attempts have been made to modify the properties of PBI by incorporating groups that make the polymer chain more flexible or other bulky units into the main or side chain to overcome the restricted polymer solubility.

Recently, ionic liquids (ILs) have attracted considerable attention in electrochemical applications. ILs are liquid molten salts at room temperature. They are composed of ions and are non-volatile substances. It is also known that ILs can be highly thermal stable at a wide temperature range. Thus, they could be good candidates for high-temperature PEMFCs (28). An example of ionic liquids that has been reported is 1-hexyl-3-methylimidazolium trifluoromethanesulfonate (HMI-Tf), its use lead to the improvement of the thermal stability and its function as a plasticizer and ion carrier enhance the conductivity of the PBI system significantly, at high temperatures. (28)

Aiming to improve solubility and proton conductivity, a novel pyridine-containing polybenzimidazole (PDA-PBI) membrane, and incorporating ether groups, was developed. It is reported the polycondensation of 4, 4'-(pyridine-2, 6-diyl-bis (oxy)) dibenzoic acid (PDA) and 3, 3'-diaminobenzidine (DAB) in phosphorous pentoxide/methanesulfonic acid (PPMA). The imparting of ether groups aims to boost the polymer solubility and flexibility. The introduction of pyridine ring is designed to increase the density of basic sites favouring the acid doping and hence improvement in proton conductivity. (27)

Furthermore, over the past few years PBI composites have been prepared with acidic surfactant like molecules (ASMs), with the purpose of improving PEM properties especially proton conductivity. Composites are obtained by homogenizing poly (4, 4'-diphenylether-5, 5'-bibenzimidazole) (OPBI) in three different ASMs namely camphorsulfonic acid (CSA), *p*-toluenesulfonic acid (PTSA) and mono-*n*-dodecyl phosphate (MDP). Mechanical reinforcement was observed, in case of composite membranes, due to an increase on the storage modulus with increasing ASM loading (29).

3. Objectives

The objectives of the present project are:

• To enhance the membrane proton conductivity by fabricating a PBI/silica functionalizedcomposite membranes for future HT-PEMFC application.

• To improve the surface interface between organic/inorganic composite membrane by applying silane coupling agent.

• To improve mechanical properties of the membrane by adding plasticizers.

• To study the effect of different coupling agents towards the performance of HT-PEMFC application by measuring their conductivities.

4. Experimental procedure

Figure 4.1 shows the experimental planning of the project. The methodology is being split into three major steps. For the preparation of OBPI/silica composite membrane, it starts with the synthesis of silica nanoparticles. Then, the surface of silica nanoparticles is functionalized using one type of amine silane coupling agent. After that, OPBI/silica composite membrane will be fabricated using 2 wt. % of loading of amine functionalized silica before it is doped with phosphoric acid. The last attempt will be devoted to prepare OPBI membranes with different amounts of plasticizers to study its influence on its conductivity properties.

In the characterization of OPBI/silica composite membrane, several techniques will be conducted to study its structural composition, thermal stability and also swelling properties. Afterwards, the proton conductivity will be measured to investigate the performance of the composite membrane.

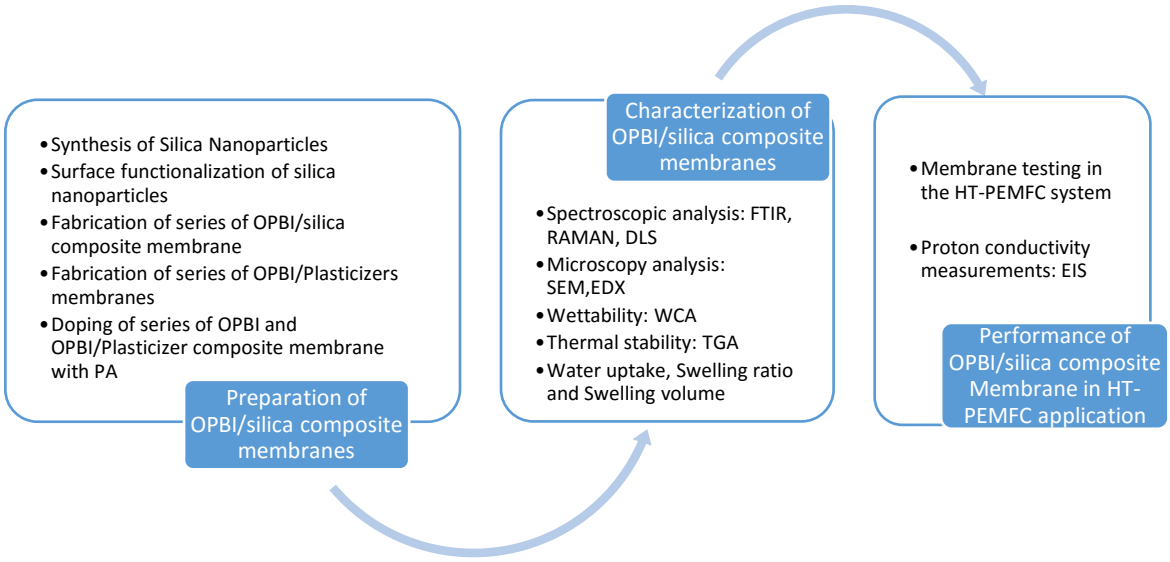

Figure 4. 1. Flow chart of the experimental procedure for the present project.

4.1. Materials

For the synthesis of OPBI, 3,3',4,4'-tetraaminobiphenyl (TAB), 4, 4'-oxybis (benzoic acid) (OBA) and orthophosphoric acid (PA, 85% H_3PO_4) were purchased from Sigma Aldrich. OPBI was synthesized in our laboratory using the method described in the following sections. Formic acid (FA, 98%), tetraethylorthosilicate (TEOS), N-(3-trimethoxysilylpropyl) diethylenetriamine (TMSPDT) and dodecylbencenesulfonic acid (DBSA) were purchased from Sigma Aldrich. All chemicals were used as received. All other reagents, unless otherwise specified, were of analytical grade and were used as received.

4.2. Synthesis of silica nanoparticles

Silica nanoparticles were prepared by hydrolysis and condensation of tetraethylorthosilicate (TEOS) in ethanol (EtOH), and in the presence of 28% ammonia acting as a catalyst. To begin with, 17,41 g of ethanol were measured and divided equally into two separate flasks. In the first flask, called EtOH A, 8,75 g of TEOS and 1,81 g of pure water were added and stirred at about 15 minutes. In the second flask, EtOH B, 0,09 g of ammonium hydroxide (28%) were poured.

Slowly, EtOH B solution was added dropwise into EtOH A solution mixture with continuous stirring, at room temperature for 24 hours. The colloidal solution was separated by centrifugation (10000 rpm; 20 min). The silica NPs obtained by the centrifugation process were washed with absolute ethanol for three times, followed by vacuum drying in an oven at 100^0C for 6 hours.

From the silica prepared on the previous step, 5,0 g were dispersed in 200 ml of toluene on a 250 ml three neck round bottom flask with nitrogen (N_2) being bubbled through vigorously for 30 min. Polyethyleneimine (PEI) (19,95 mol) was added dropwise and the reaction mixture was stirred at room temperature for 10 minutes before it was heated to 110^0C. The mixture was then refluxed for 12 hours.

After the aforementioned period, the suspension mixture was separated by using again centrifugation (10000 rpm; 20 min). The functionalized silica was washed with absolute ethanol for three times, followed by drying vacuum in the oven at 100^0C for 6 hours. When the sample was dried, it was stored in an appropriate container.

4.3. Synthesis of OPBI

For the OPBI synthesis, 2,1951 g (0,0085 mole) of 3,3',4,4'-tetraaminobiphenyl (TAB) and 1,8213 grams (0,0085 mol) of 4,4'-oxybis(benzoic acid) (OBA) were mixed with orthophosphoric acid (PPA)(115%; 100 g) are placed in 250 ml three-necked, round bottom flask equipped with reflux condenser with an inlet of nitrogen gas flow.

The reaction mixture was stirred with a mechanical overhead stirrer (50 rpm) and a slow stream of purged nitrogen gas (0,55 bar) was maintained throughout the reaction. The mixture was then placed in an oil bath, and the temperature was controlled with a temperature controller at 190-220^{0}C for 26 hours. The reaction mixture became more viscous and a dark brown colour solution appeared at the end of the polymerization time.

The mixture was poured into a beaker with double-distilled water and a brown powder precipitated. The mass was then pulverized and neutralized with sodium bicarbonate (5%), washed thoroughly with water, and finally dried in a vacuum oven for 24 hours at 100^{0}C to obtain the dry OPBI powder.

4.4. Membrane forming and doping

Polymer films preparation

In order to prepare 1% of OPBI solution, in a small sample container, approximately 20 mg of OPBI powder must be weighted. By using a micropipette, 2 mL of formic acid (FA) were added into the flask. The solution is then placed in a water bath at 40ºC and stirred by using a magnetic stirrer until the OPBI powder complete dissolution.

Since the OPBI powder was dissolved, the solution was poured onto a Petri dish to cast the membrane after the acid-water evaporation. For this step, the Petri dish was covered with aluminium foil with some small holes and left under fume hood to the slowly evaporation of the solvent, under room temperature for overnight. After the drying process, the OPBI film was peeled out from the Petri dish and stored in a glass container and desiccator, for further use.

For the OPBI/Si-PEI film fabrication (physical mixing membranes composed by OPBI and Si-PEI NPs), 1 ml of FA measured with a micro pipette was added into a small glass sample vial. 20 mg of OPBI dry powder was weighted and added into the glass sample vial containing FA. The mixture was stirred and placed in a water bath (40^{0}C) to solubilize the OPBI polymer in FA completely. In the meantime, in another small glass sample vial, 1 ml of FA and 20 mg of Si-PEI NPs were added and mixed together until the complete dissolution, by using ultrasonic bath (15 min). Then, the first solution containing

OPBI and the second, containing Si-PEI NPs, were mixed and the film casting was carried out with the same procedure than the pure OPBI films, described above. This film was called OPBI/Si-PEI.

For the preparation of OPBI membrane with dodecylbencenesulfonic acid (DBSA), acting as dopant and possible plasticizer agent, the procedure is illustrated in the *Figure 4.2*.

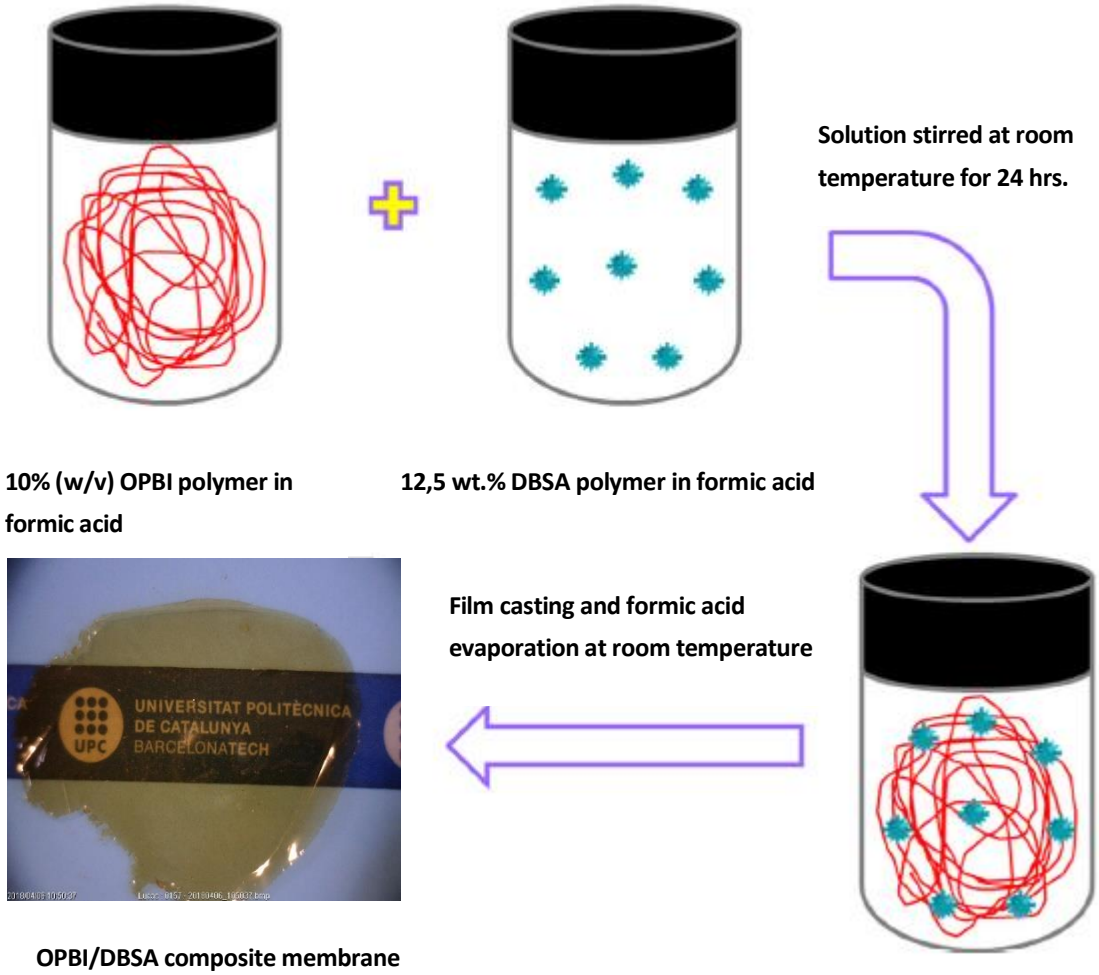

Figure 4. 2. Schematic representation for the preparation of OPBI composite membrane with acidic surfactant like molecule (ASM). Adapted from reference (29)

Doping process

The thoroughly vacuum-dried series of OPBI membranes were immersed in phosphoric acid viscous liquid (85%) for 7 days to get freestanding PA doped films. After 7 days, the membranes were taken out from phosphoric acid (PA) bath, quickly wiped the surface to eliminate the excess of PA, and then stored for further analysis in a desiccator under vacuum conditions (12). To get the percentage of PA incorporated, membranes were weighted before the PA bath and after the doped polymer

membranes were dried at 110^{0}C under vacuum until an unchanged weight is reached. The results were expressed according to the method described in the section 4.5.5. (swelling properties) (14).

4.5. Characterization techniques

4.5.1. Spectroscopic characterization

FTIR is a sensitive technique applied in analytical chemistry for the characterization of molecules and functional groups. It has proved to be useful and a popular tool in identification and characterization of organic materials. The technique is based on the fact that, molecules absorb specific frequencies that are characteristic of their structure, these absorptions are related to the strength of the bond. (30)

In this project, **infrared spectra** (FTIR) were measured in the range of 600-4000 cm^{-1} with a FTIR 4100 Jasco spectrophotometer coupled to an attenuated total reflection (ATR) accessory with a diamond crystal (Specac model MKII Golden Gate Heated Single Reflection Diamond ATR) (*Figures 4.3* and *4.4*). The samples were evaluated in film shape with a size of 3x3 mm^2, approximately.

Figure 4. 3. Jasco 4100 spectrometer

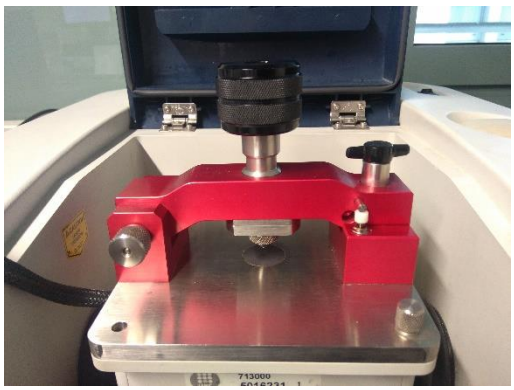

Figure 4. 4. ATR accessory

RAMAN spectroscopy is a photonic analysis technique that allows the identification and characterization of a material, regardless of its nature (organic or inorganic) and its physical state

(gas, liquid or solid). The technique is based on the procurement of the radiation dispersed in an inelastic way by a material when a beam of monochromatic light impinges on it. The phenomenon that occurs, with characteristics inherent to the molecular composition and crystal structure of the irradiated sample, is called the Raman effect. (31)

RAMAN spectra of the samples studied here were obtained through Renishaw InVia confocal Raman microscope (*Figure 4.5*), at 785 nm of laser excitation, with an exposure time of 1 s, a laser power of 0.1%, 3 accumulations and in the Raman shift range of 600-1800 cm^{-1}. The samples were evaluated in film shape with a size of 1,5 cm x 7 mm, approximately.

Figure 4. 5. Renishaw InVia confocal RAMAN microscope

Scattering is a general physical process in which some forms of radiation changes its direction and, on occasion, its frequency after interacting with the medium. In light scattering process when a light beam incises in a determinate frame the total number of photons is unaltered, but the number going in forward direction decreases due to redirection of light from scattering interaction. In other words, when light impinges on matter, the electric field of the light induces an oscillating polarization of electrons in the molecules and these molecules provide a secondary source of light and subsequently scattering light. The frequency shifts, the angular distribution, the polarization and the intensity of scattered light are determined by the size, shape and molecular interaction in the scattering material. (32)

Dynamic light scattering (DLS) NanoBrook Omni Zeta Potential Analyzer (from Brookheaven Instruments) (*Figure 4.6*) was employed for particle size measurements using 10 mg/L of Si-PEI dilute aqueous solutions. The samples were in the form of dispersed particles in liquid solution.

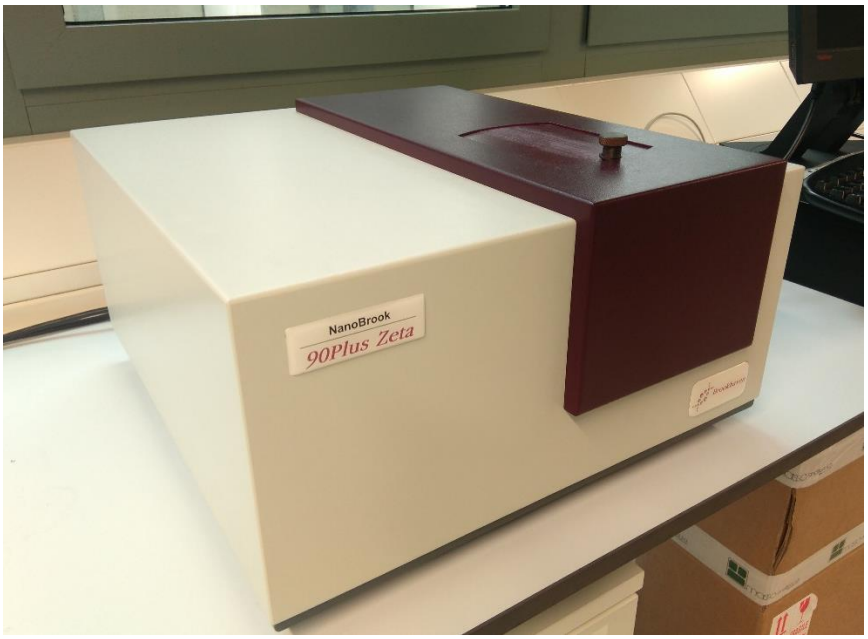

Figure 4. 6. DLS NanoBrook Omni Zeta Potential Analyzer

4.5.2. Microscopy analysis

The scanning electron microscope is a powerful instrument that permits the observation and characterization of heterogeneous organic and inorganic materials and surfaces on a specific scale. The area to be examined is irradiated with a finely focused electron beam, producing secondary and backscattered electrons signals that can be used to examine many characteristics of the sample: composition, surface, topography, crystallography, and others.(33)

Inspection of the cryo-fractured surfaces of OPBI films, employing liquid nitrogen, was conducted by **scanning electron microscopy (SEM)** using a Focus Ion Beam (FIB) Zeiss Neon 40 instrument (Carl Zeiss, Germany) (*Figure 4.7*) operating at 5kV, equipped with an EDX spectroscopy system. Films were covered with conductive carbon coating, by using Mitec K950 Sputter Coater, before SEM analysis. The samples were used in film shape, with a size of 3x4 mm^2, approximately, and varied thicknesses.

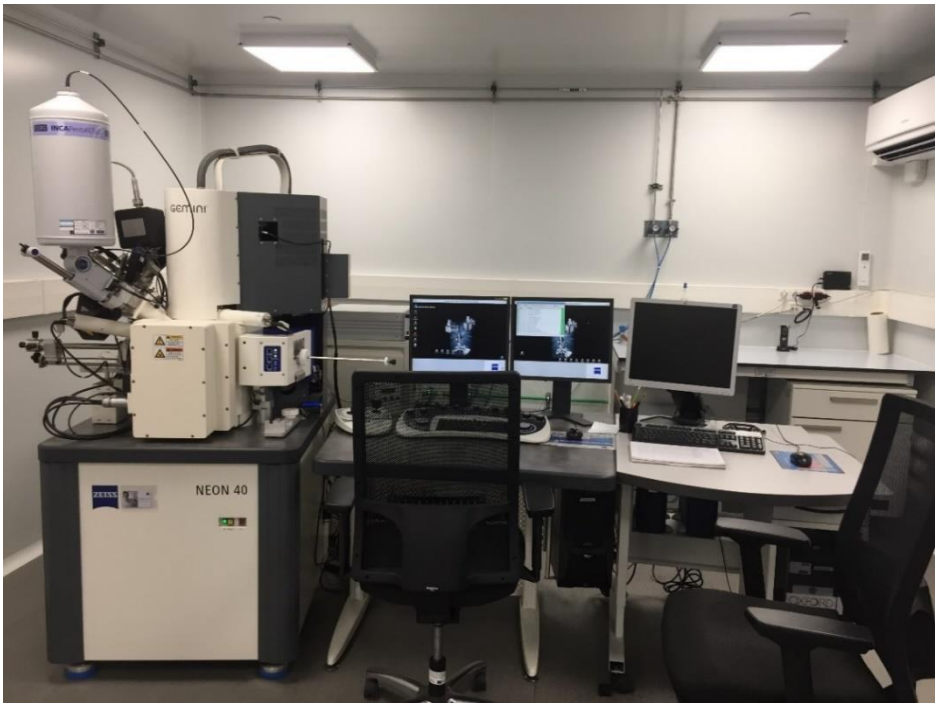

Figure 4. 7. Focus Ion Beam (FIB) Zeiss Neon 40 instrument

4.5.3. Wettability

When a gas and liquid, separated by their common interface, encounter a solid surface, the contact line between the three phases is called the common line (CL), the contact angle (θ) is the one between the liquid-solid, and liquid-gas interfaces, *Figure 4.9*. If θ is lower than 90^0, the surface is called hydrophilic, whereas if θ is greater than 90^0, the liquid is non-wetting, so the surface is called hydrophobic.(34)

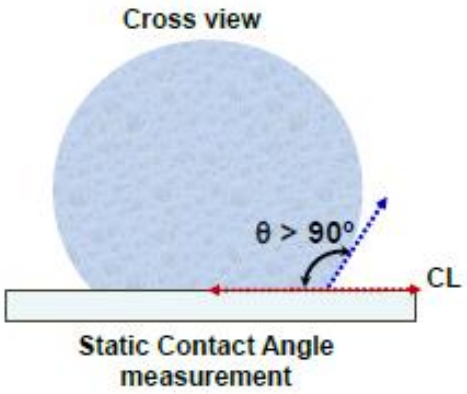

Figure 4. 8. Static contact angle measurement (34)

Contact angle measurements were performed by employing OCA 20 (DataPhysics Instruments GmbH, Filderstadt) equipment (*Figures 4.10* and *4.11*) and using the sessile drop method at room temperature. For the static contact angle (sCA) measurements, 0,500 µL droplets of distilled water were dispensed on the respective surfaces. The contact angle values (software SCA 20) were obtained as the average of ten independent measures for each sample, which was flat films with 1,5x1,5 cm^2 of area.

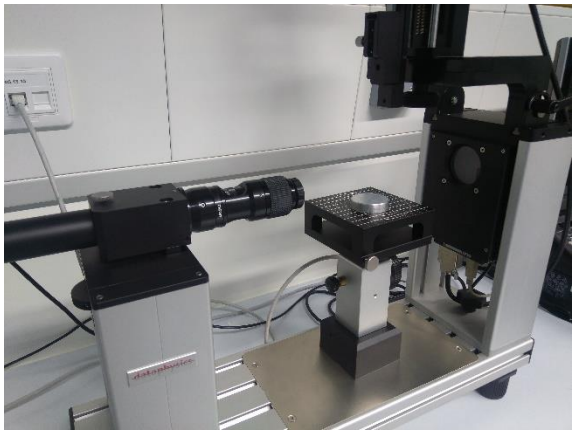

Figure 4. 9. OCA 20 equipment for the measurement of WCA (a)

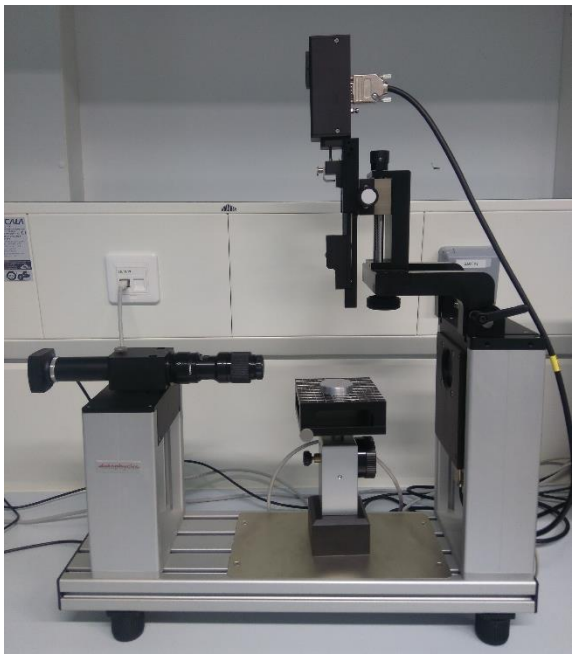

Figure 4. 10. OCA 20 equipment for the measurement of WCA (b)

4.5.4. Thermal stability

Thermogravimetric analysis (TGA) is a method of thermal analysis in which the mass of a sample is measured over time as the temperature changes. This measurement provides information about physical phenomena, such as phase transitions, absorption and desorption; as well as chemical phenomena including chemisorptions, thermal decomposition, and solid-gas reactions. (35)

Thermogravimetric analysis (TGA) was carried out with a DTA1600 thermogravimetric analyser of TA Instruments (*Figures 4.12* and *4.13*) at a heating rate of 10^0C/min, under argon atmosphere, from 20^0C to 1100^0C. The polymer mass required for this experiment was at about 15 mg in powder shape.

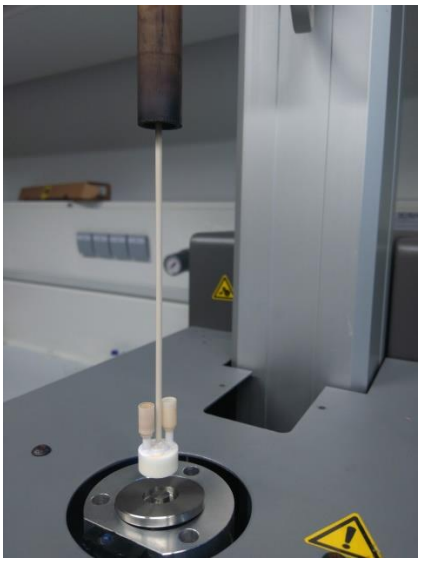

Figure 4. 11. Detail of the thermogravimetric analyser

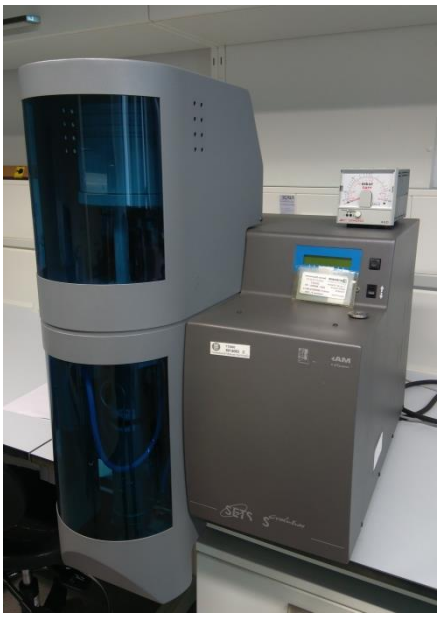

Figure 4. 12. DTA1600 thermogravimetric analyser

4.5.5. Water uptake, swelling ratio and swelling volume measurements in water and PA

For **water uptake**, **swelling ratio** and **swelling volume measurements** in water and acid, the membranes, with variable dimensions (3-24 mm), were first dried thoroughly in a vacuum oven at 100^0C for 3 days. Similar sized pieces of membranes were cut in triplicate and their weights, dimensions and thickness noted. They were then immersed in distilled water for 3 days (for measurements in water) and in PA for 3 days (for measurements in acid). After the specified period, the wet membranes were quickly wiped to remove the surface water (or acid) with filter paper and their weights, dimensions and thickness were noted again. Water uptake, swelling ratio and swelling volume were calculated as:

$$\text{Water Uptake} = \frac{W_w - W_d}{W_d} x100\% \qquad \textit{(Eq, 4.1)}$$

$$Swelling Ratio in PA \,\&\, water = \frac{L_w - L_d}{L_d} x100\% \qquad \textit{(Eq, 4.2)}$$

$$Swelling Volume in PA \,\&\, water = \frac{V_w - V_d}{V} x100\% \qquad \textit{(Eq, 4.3)}$$

Where W_w,L_w and V_w are the weight, length and volume of the wet membranes, respectively and W_d, L_d and V_d are the weight, length and volume of dry membranes, respectively. These measurements were carried out in triplicate, independently, with three similar sized pieces of the membranes to check for reproducibility, and the average values were calculated.

4.5.6. Proton conductivity measurement

One of the most modern impedance analysis systems is the Electrochemical Impedance Spectroscopy or EIS. It is a relatively new and powerful method of characterizing electrical properties of materials and their interfaces with electronically conducting electrodes. It can be used to investigate the dynamics of bound or mobile charge in the bulk of interfacial regions of any kind of solid or liquid material: ionic, semiconducting, and mixed electronic-ionic or dielectrics.

Electrochemical impedance is measured via the current through an electrochemical cell, to which a small excitation AC potential is being applied. The mathematical analysis is done using Fourier series. The EIS experiment involves the application of a sinusoidal electrochemical perturbation (potential or current) to the sample that covers a wide range of frequencies. The multi-frequency excitation allows

the measurement of several electrochemical reactions that take place at different rates and the measurement of the capacitance of the electrode. The most common and standard procedure is to measure the impedance applying a single-frequency voltage or current to the interface of the electrode, and measuring phase shift and amplitude (real and imaginary parts) of the resulting current at said single-frequency, using either analogue circuits or fast Fourier transform (FFT) analysis. (36)

Electrochemical Impedance Spectroscopy (EIS) measurements were performed using a capacitor cell and an AUTOLAB-302N potentiostat/galvanostat (*Figures 4.14-4.16*) operating between the frequency range of 10^4 Hz and 10^{-2} Hz and 10 mV of amplitude for the sinusoidal voltage. The volume of the cell is defined by a 15 mm inner diameter and a 2 mm inner depth. The pressure is kept constant and defined by the maximum limits of screws used to close the probe arrangement, *Figure 4.17*. For the assays, the films were previously cut into disks (area = 1.766 cm^2); dry film thickness (DFT) values were measured with a Neurtek Mega-Check pocket FE device. (6)

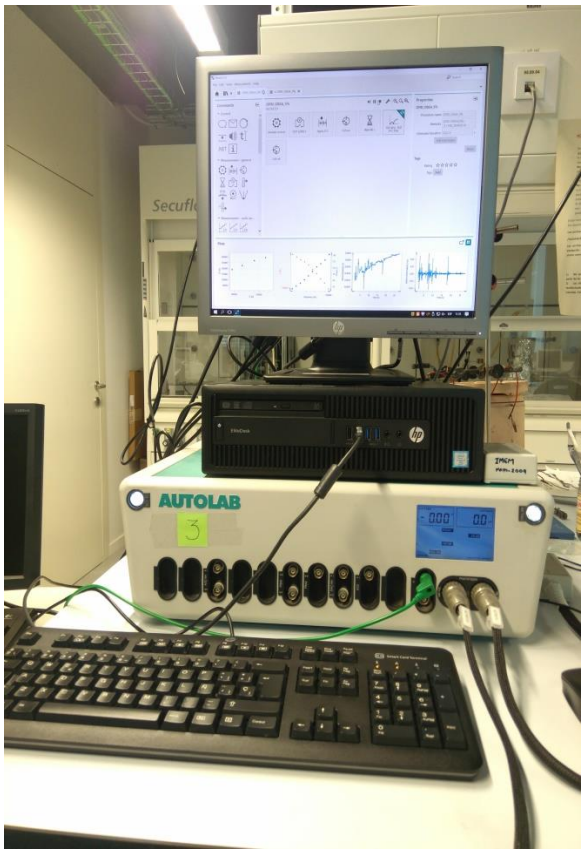

Figure 4. 13. Autolab-302N potentiostat

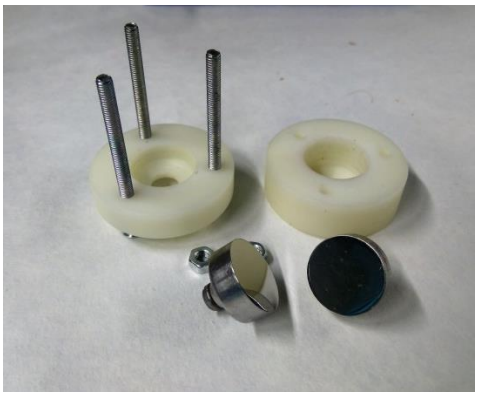

Figure 4. 14. Capacitor cell

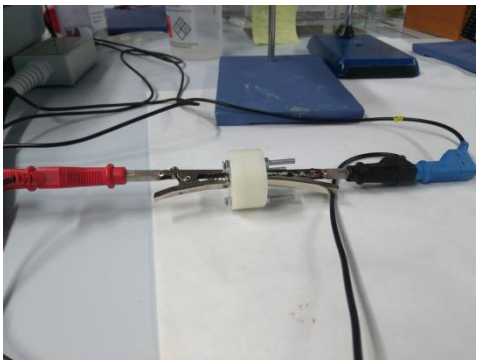

Figure 4. 15. Cell assembly

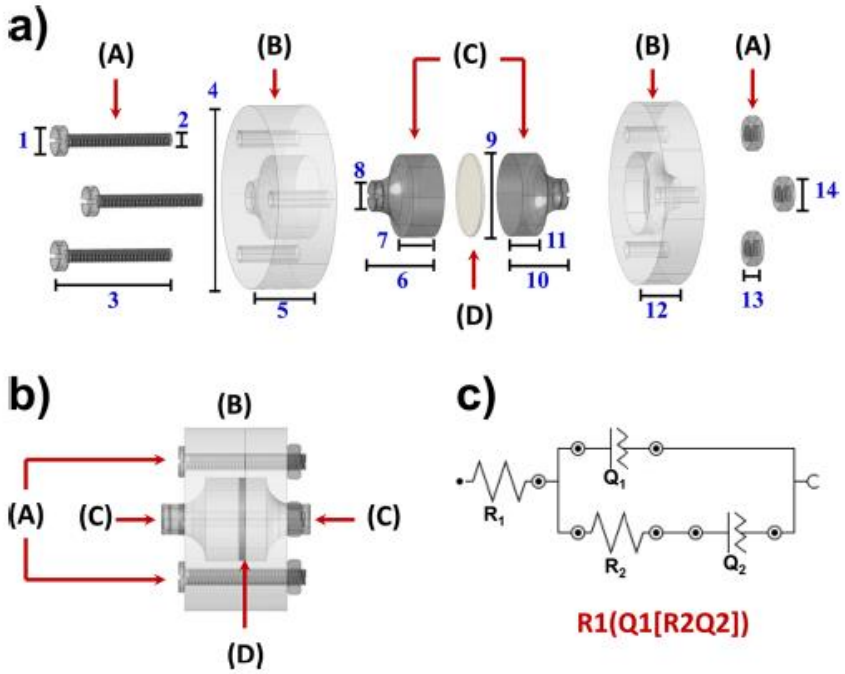

Figure 4. 16. Schematic representation of the cell geometry and membrane arrangement used in the present study: (a) 3D open view of the individual parts of the through-plane impedance cell with their corresponding size (1, 5,40 mm; 2, 2,60 mm; 3, 22,10 mm; 4,32,95 mm; 5, 11,15 mm; 6, 12,00 mm; 7, 5,70 mm; 8, 9,40 mm; 9, 15,00 mm; 10, 11,50 mm; 11, 5,70 mm; 12, 7,70 mm; 13, 2,35 mm;14, 5,45 mm.) (b) Configuration of the closed arrangement probe. (c) Equivalent electrical circuit.(6)

The acid loaded membrane was cut into a disc shape and mounted onto the in house built conductivity cell. The membranes were dried at 100°C by heating and holding at 100°C isothermally for 2 hours to remove the water from the membrane. The membrane samples were cooled in a vacuum oven and taken out before conductivity measurement in an effort to keep the samples dry. The conductivities of the samples were obtained from the direct- current potential difference between the two inner electrodes. The conductivity was calculated with the following equation:

$$\sigma = \frac{D}{RBL} \qquad \textbf{(Eq, 4.1)}$$

where, σ is the proton conductivity (S/cm), D is the distance between the electrodes, B and L are the thickness and width of the membranes respectively and R is the resistance obtained from Nyquist plots.(16) For the high temperature assays, the samples were left in a vacuum oven for 48h to stabilize before EIS analysis.

5. Results and discussion

The pristine OPBI films, obtained by direct casting on Petri dishes, were characterized and compared to the OPBI composites obtained with silica nanoparticles, as well with the DBSA plasticizer.

In the first part of this section, we discuss the results obtained with the filler synthesis and the chemical functionalization with PEI molecules. Further, in the second part, the complete characterization of the physical-chemical properties of the membranes synthesized will be approached.

5.1. Synthesis of silica-PEI nanoparticles

The synthesis of Si-PEI NPs was carried out by using the Stöber method, reported elsewhere, (37). The objective was to synthesize nanoparticles between 40-80 nm. In fact, the particle size distribution is relevant for the good dispersion of the filler inside the OPBI polymer matrix. Nowadays, there is an extended knowhow to prepare them and the research community recognizes the benefits of finer particle size in the materials performance. Thus, measurements of the primary silica particles and the silica modified with PEI were taken into account with two techniques: Dynamic Light Scattering (DLS) and Scanning Electron Microscopy (SEM). In the first procedure, que NPs were previously dispersed in a diluted aqueous solution and were sonicated with probe-type sonication for 5 min in ethanol to disperse it evenly. The particles size distribution was found to be between 100 - 150 nm (*Figure 5.1*), higher than that expected. This is, probably caused by some aggregation between the modified silica particles causing the particles size distribution to be at a higher range. However, the difference of particle size distribution, before and after sonication, is remarkable. The primary particle size can be close to micrometres (*Figure 5.1a*), whereas the sonicated particles can be reduced to hundreds of nanometres (*Figure 5.1b*). This means a reduction of about 10X the initial size. Perhaps, by increasing the amount of sonication time, it could reduce the aggregation between the silica particles and give a better particles size distribution reading. We should mention that fillers being highly aggregated and agglomerated have particles size distributions in the tens to hundreds of micrometres range. Therefore, we consider Si-PEI NPs well stabilised for further addition to the OPBI/FA solutions.

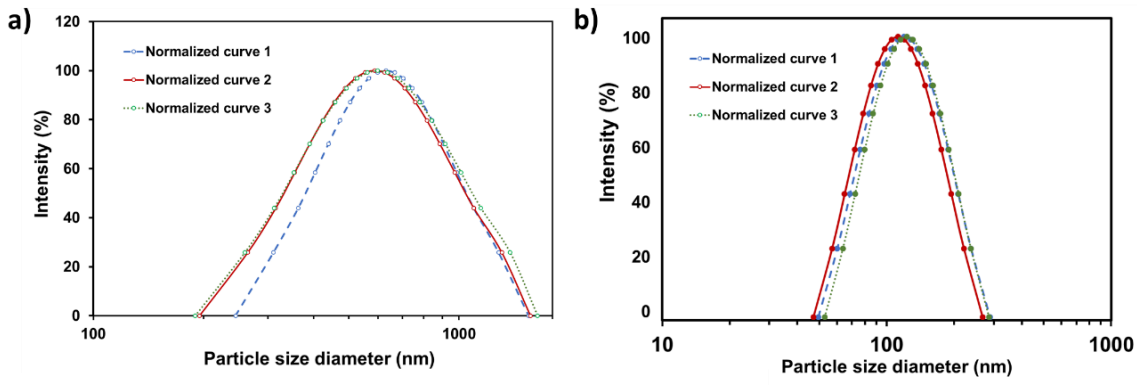

Figure 5. 1. a) DLS results showing the volume percentage of particles towards particle size diameter of Si-PEI filler, before sonication process; and b) particle size distribution of Si-PEI filler, after the sonication process in EtOH for 5 min.

When reducing particle size, it cannot be overemphasized that stability must still be maintained. Small particle size implies high surface contact area, *i.e.* high surface energy that tends to poor stability. Therefore, the filler sonication and its addition to the OPBI/FA solution must be an almost

concomitant activity. The SEM images (*Figure 5.2*) demonstrate the above-mentioned effect of sonication on the particle size reduction and can be seen the ease capability of Si-PEI particles to aggregate.

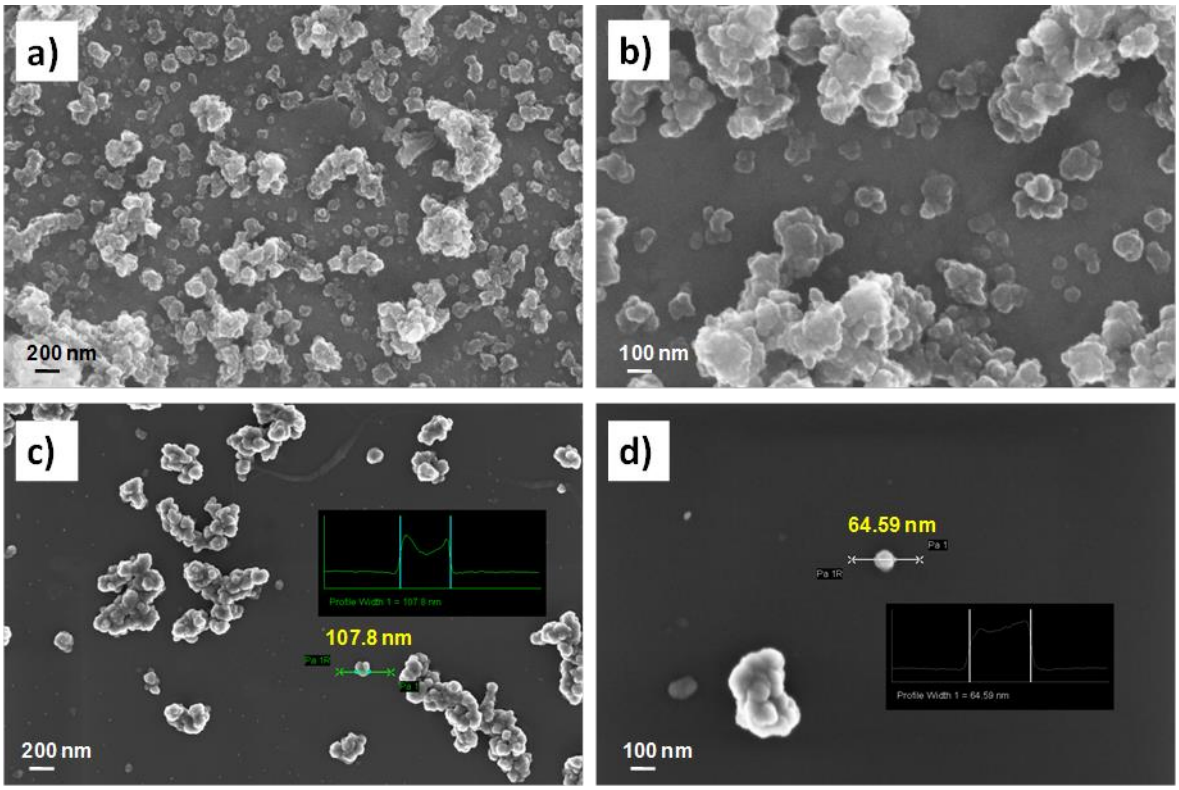

Figure 5. 2. SEM micrographs of Si-PEI NPs, before sonication: a) low magnification, b) high magnification; and after sonication process: c) low magnification and d) high magnification. Values inset are related to one or two individual particles.

The chemical composition of Si-PEI NPs was checked by FTIR. Therefore, the *Figure 5.3* compares the absorption bands for the pristine SiO_2-OH particles and SiO_2-OH after functionalization (named Si-PEI). The absorption bands between 1260 – 1050 cm^{-1} is assigned to the Si-O-Si asymmetric stretching vibration while at 950 cm^{-1} referred to the asymmetric vibration of Si-OH, there is another absorption band at 750 cm^{-1} that corresponds to the vibration of Si-O. Similar absorption bands of the silica nanoparticles has been reported elsewhere (38)(39).The main difference between the two IR spectra could be observed in *Figure 5.3b.* The absorption bands between 1454 cm^{-1} and 2820-2980 cm^{-1} are assigned to the vibration corresponding to the methylenes ($–CH_2$), characteristic of the structure of the Si-PEI NPs. It must be highlighted the wide band that appears between 3000-3500cm^{-1} that corresponds, in the case of the SiO_2-OH to the vibration of the -OH and in the case of the Si-PEI, which is slightly wider and more intense, corresponds to the vibration of –NH.

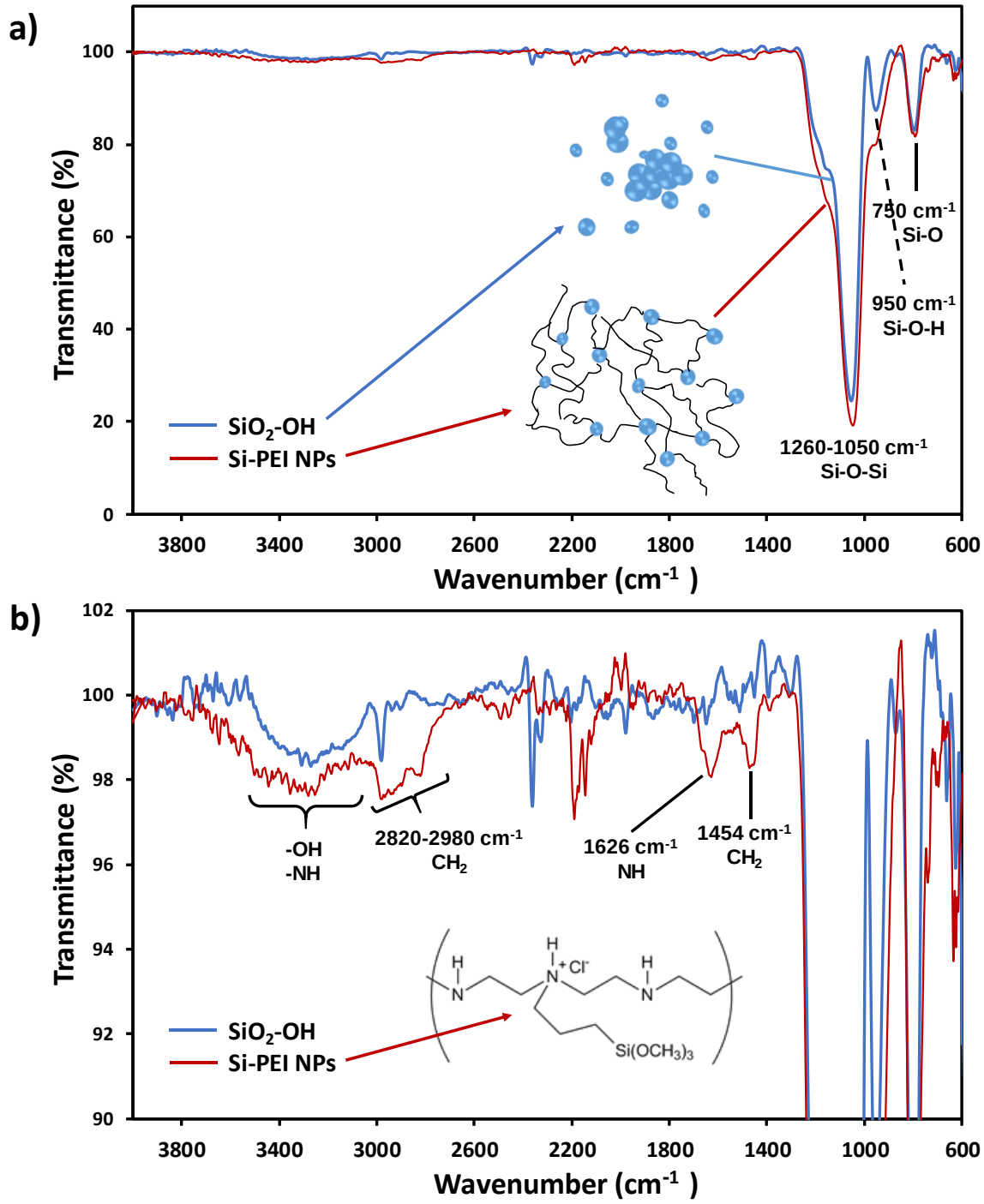

Figure 5. 3. Infrared spectra of Si-OH pristine particles and Si-PEI nanoparticles, functionalized with polyethyleneimine: a) FTIR spectra from 0 to 100% of transmittance showing the main absorption bands from silica inorganic filler, and b) FTIR spectra from 90 to 100% of transmittance to check the presence of NH and CH_2 groups onto silica surface.

As noted above, it has been possible to obtain functionalized silica nanoparticles with the needed size, as it was required for the following section of this project.

5.2. Synthesis of OPBI

The present section will be based on the description of the most noteworthy observations during the preparation of the polymer films.

As mentioned in previous sections, the method for creating the membranes was by casting the solution directly on Petri dishes. After casting the membrane, it was left at room temperature for one-two days and then stored in a desiccator at 100^0C to eliminate the excess of solvent (FA or PA). After this process, the films had to be cut in equal pieces to proceed with their characterization, which was a mayor issue due to their **fragility**. Comparing the pristine OPBI film (*Figures 5.4-a,c*) with the OPBI composite (*Figures 5.4-b,d*), before and after doping, it can be seen that the first ones are transparent whereas the last ones are opaque, despite a very low concentration of silica NPs were introduced. In particular, OPBI/Si-PEI film was the one that presented the worst mechanical integrity, turning into small pieces when they were cut, immersed or simply dried (*Figures 5.4b and 5.4d*). Thus, pointing out the contrary effect than that reported in the literature (see introduction section). Additionally, it should be noted that these films became less brittle when they were doped with phosphoric acid, evidencing that these molecules actuate as a kind of liquid plasticizer for the polymer matrix. It will also been seen later, with the cross-section SEM analysis.

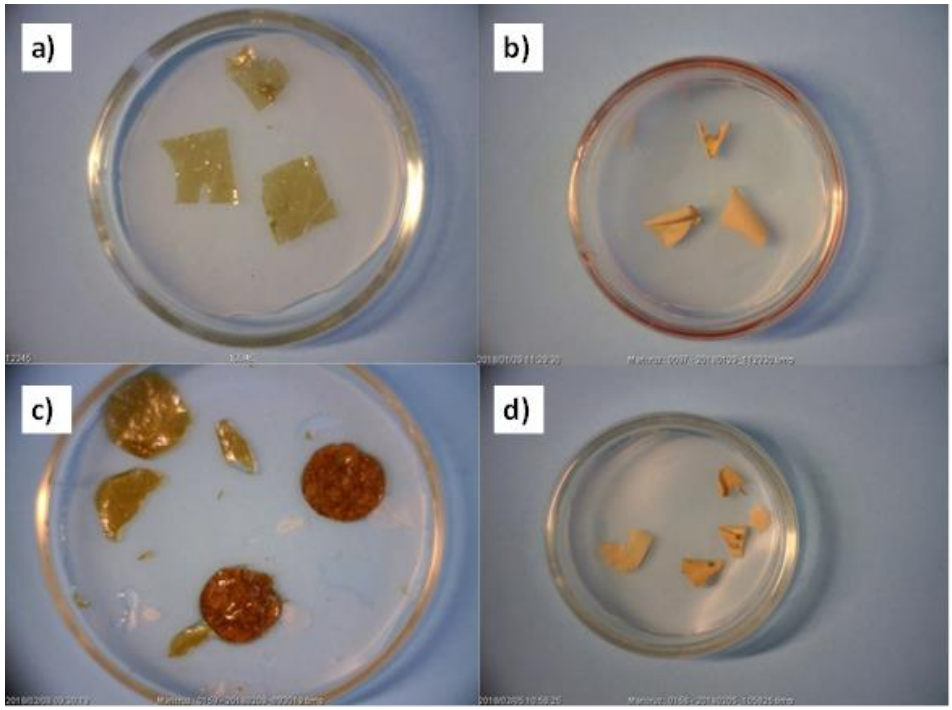

Figure 5. 4. OPBI membranes after swelling measures: a) OPBI membrane before swelling analysis; b) OPBI/Si-PEI membrane after swelling analysis; c) OPBI-doped disc membranes after swelling analysis; d) OPBI/Si-PEI membrane after swelling analysis

Seeing the brittleness of the OPBI/Si-PEI undoped films, one possible solution to overcome the problem was to convert the samples into **powder** and to **compact** them, with a hydraulic press; to create **discs** with more precise geometry (*Figure 5.5*). However, it did not turn out to be a good solution, since the powder, being compacted, had serious difficulties to preserve the disc form, when immersed in a solvent; hindering swelling measures as well as its subsequent doping..

Figure 5. 5. OPBI compressed discs

Based on the unsuccessful outcome of the previous experiment, plasticizer addition was approached. Tests were performed to ascertain proper DBSA concentration in the OPBI membrane. Therefore,

weight mass varying between 12,5 wt.% to 50 wt. % was tried. As can be seen in *Figure 5.6a*, with the highest content, the film was not even been formed, leaving the material in powder shape adhered to the Petri dish. In *Figure 5.6b,* the film (OPBI/DBSA (37,5 wt.%) was successfully obtained but it was still very fragile. Finally, the optimal content was found to be 12,5 wt. % of DBSA acid. It was possible to create an integral film (*Figure 5.6c*), with better mechanical properties in an undoped state than the pristine OPBI or the OPBI/Si-PEI membranes.

Figure 5. 6. OPBI tests with DBSA plasticizer: a) OPBI/DBSA (50%); b) OPBI/DBSA (37.5 %); c) OPBI/DBSA (12.5 %).

Despite the issues raised with the membrane preparation, it was possible to perform all the necessary tests for the total characterization of the films.

5.3. Characterization of the OPBI films

During the following section, the most remarkable results of the characterizations carried out are explained, for instance: FTIR and RAMAN spectroscopic analyses, SEM microscopy evaluation, wettability tests, thermogravimetric study, swelling tests and proton conductivity measurements.

5.3.1. Spectroscopy characterization

The **FTIR spectra** of each pair of films: OPBI, OPBI/Si-PEI and OPBI/DBSA (12,5%) (doped and undoped) generated are included in the *Figures* 5.7-5.9.

In the *Figure 5.7*, we can appreciate a comparison between the OPBI film undoped and the one doped. One of the main characteristic of the infrared from the undoped films is their broad and less intense absorption bands compared with the doped films. Some of the absorption bands in OPBI doped films are very sharp and well-defined, which main peaks correspond to the characteristic band of phosphoric acid between 3000-2500 and between 1200-500 cm^{-1}.

As reported in previous works, OPBI shows three characteristic peaks at 3413, 3144 and 3066 cm^{-1} attributed to non-hydrogen bonded free N-H groups, self-associated hydrogen-bonded N-H groups and stretching modes of aromatic C-H groups, respectively (16).

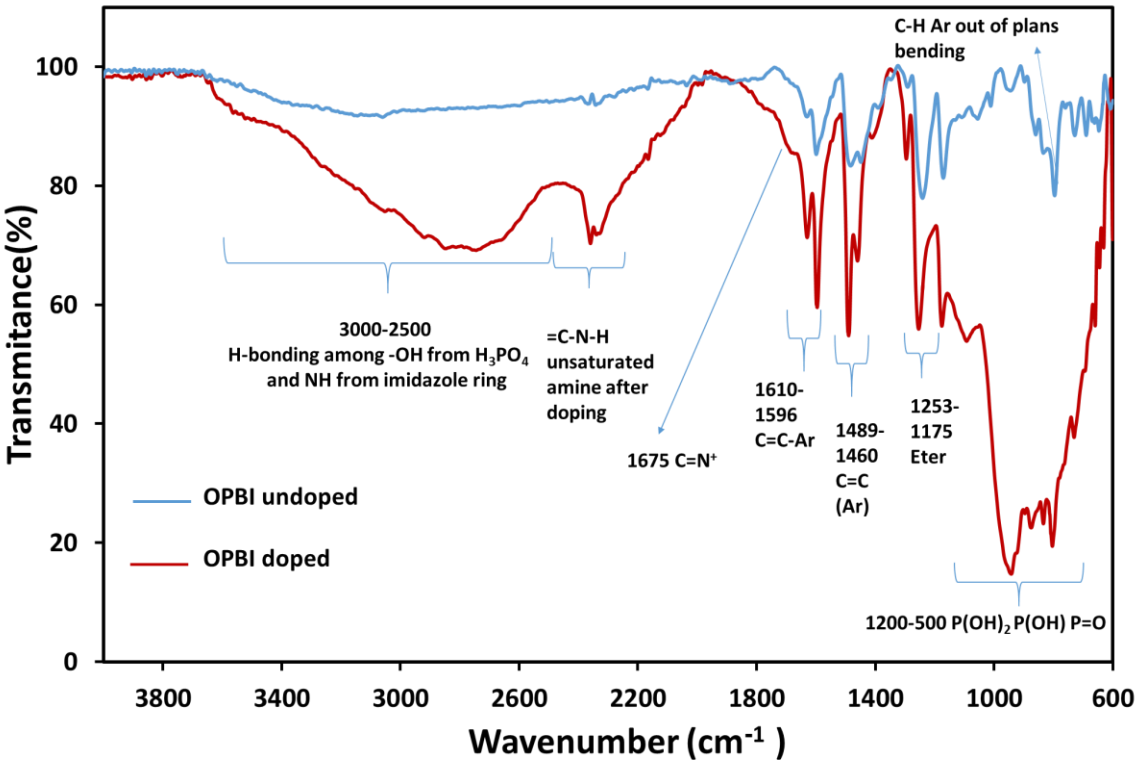

Figure 5. 7. Infrared spectra of OPBI undoped and doped films

The infrared spectra of OPBI/Si-PEI films is presented in the *Figure 5.8*. The peaks at 1273, 1169, 1053 and 794 cm^{-1} could be assigned to the silica nanoparticles, as seen in the *Figure 5.3* from previous sections. On keen observation, we see that the intensity of peaks of =C-N-H functionality (at 2300 cm^{-1}) decreases in the silica membranes, suggesting the formation of hydrogen bonds between amine groups of polymer and functional groups of the Si-PEI.(12)

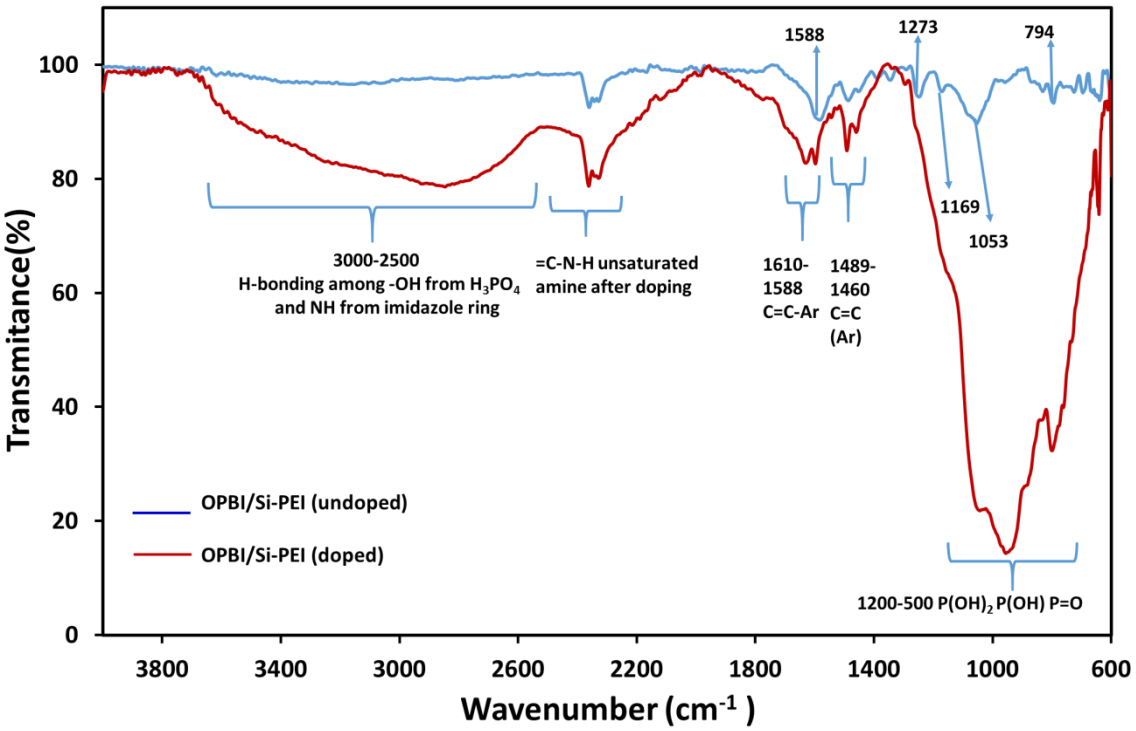

Figure 5. 8. Infrared spectra of OPBI/Si-PEI undoped and doped films

The infrared spectra of OPBI films with 12,5 wt.% of DBSA molecules is shown in the *Figure 5.9*. The peaks at 3393, 2916, 1031 and 1006 cm^{-1} could be assigned to O-H stretching, C-H stretching of $–CH_2$, S=O stretching and >CH stretching of benzoic rings in DBSA molecule, respectively. Some of these peaks were also observed in the doped films but these bands are collapsed with that from phosphoric acid absorption bands, in the wavenumber between 3000-2500 cm^{-1} and between 1200-500 cm^{-1}.

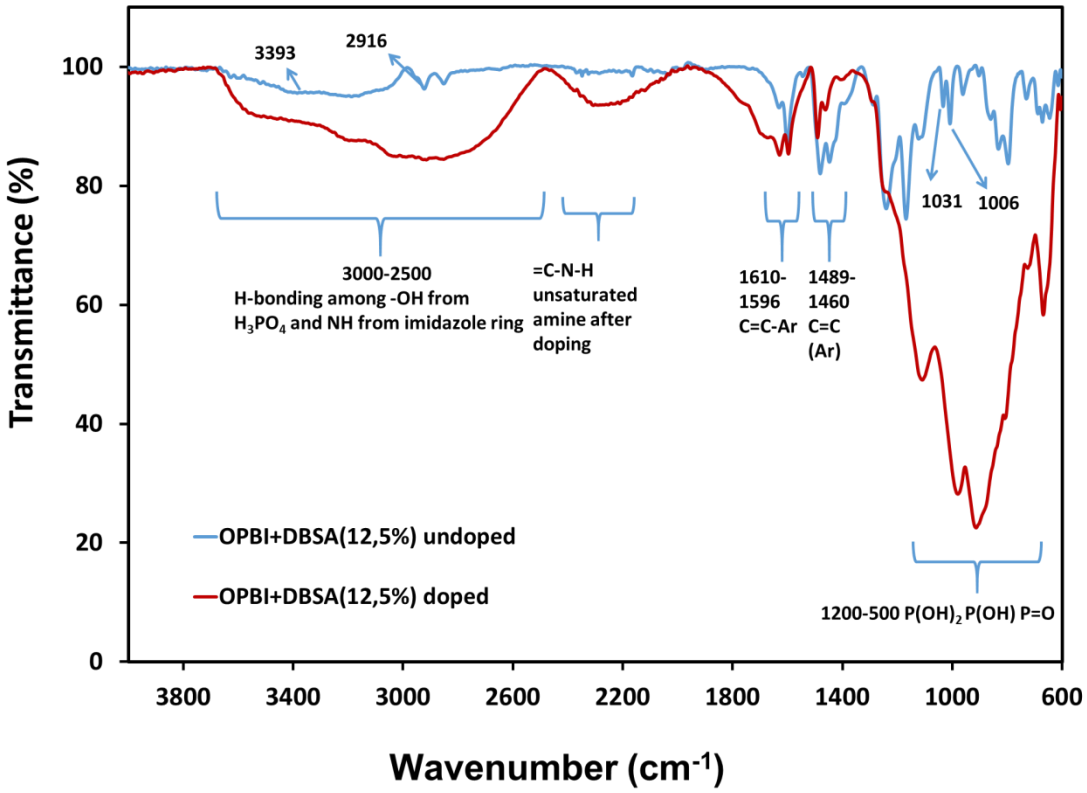

Figure 5. 9. Infrared spectra of OPBI+DBSA (12,5%) undoped and doped films

Raman spectroscopy was employed to confirm the main absorption bands found in the infrared analysis.

The **RAMAN spectra** of each pair of films: OPBI (doped and undoped), OPBI/Si-PEI (doped and undoped) and OPBI/DBSA (12,5%) undoped, are included in the *Figures 5.10 - 5.12*.

The three spectra of the undoped films show very similar absorption bands due to the low amount of silica-PEI nanoparticles (less than 2 wt.%) and plasticizer present in the OPBI/Si-PEI and OPBI/DBSA films, respectively. However, small differences on the late can be found. For this reason, the first discussion will be related to these three samples. The peaks at 1616, 1577 and 1548 cm^{-1} could be assigned to C=C stretching from the aromatic compounds. They represent the most intense bands in the Raman spectra. The last one (1548 cm^{-1}), as well as the peak at 1460 cm^{-1}, could also be assigned to the C=N stretching and, to end up, the peak at 964 cm^{-1} could be assigned to C-H vibration of the benzene ring.(14) On the other hand, by comparing these spectra with doped ones, we can appreciate new and broad absorption bands, in the range of 1300-1500 cm^{-1}.

As for the comparison of undoped and doped membranes, it is reported in *Figure 5.13* the RAMAN spectra of the pure polyphosphoric acid. In this image it is remarkable the intensity of the peak at

1372 cm^{-1}, which represents the P=O vibrations. Another peak to take into account should be the P-OH vibration at 911 cm^{-1}. Comparing this spectrum with that of *Figures 5.10 and 5.11*, we can also see a wide bands between 1337-1397 cm^{-1} that proves the acid is trapped inside the OPBI films.

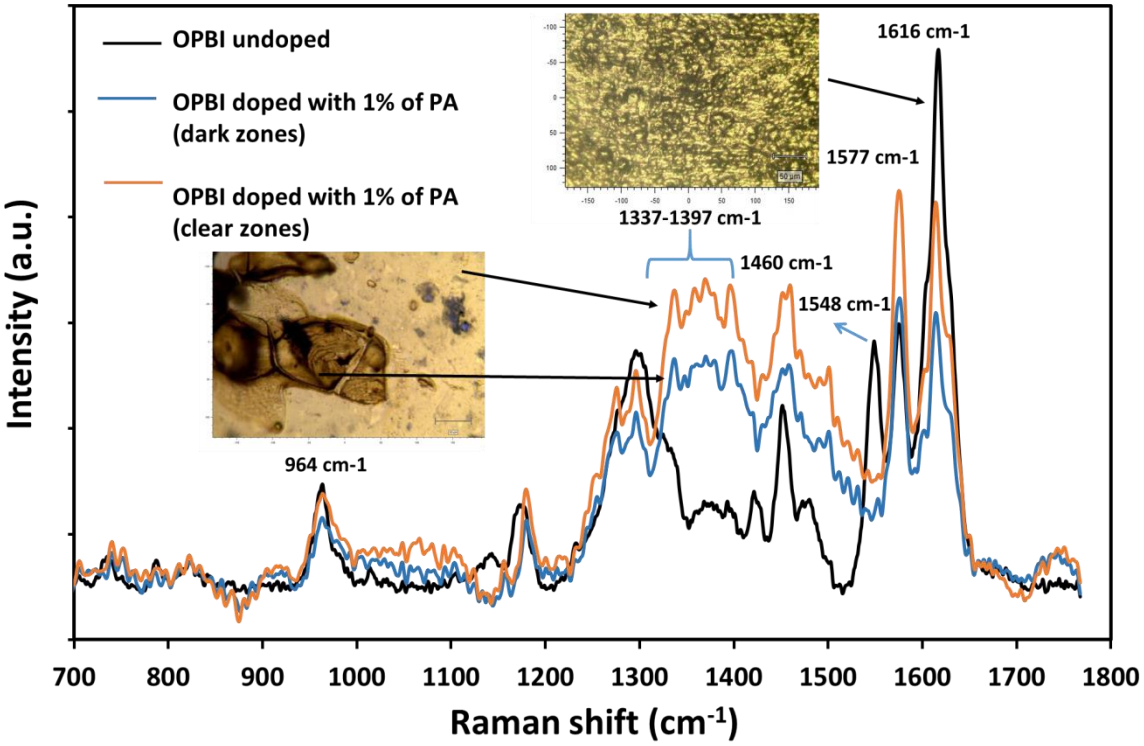

Figure 5. 10. Raman spectra of OPBI undoped and doped films

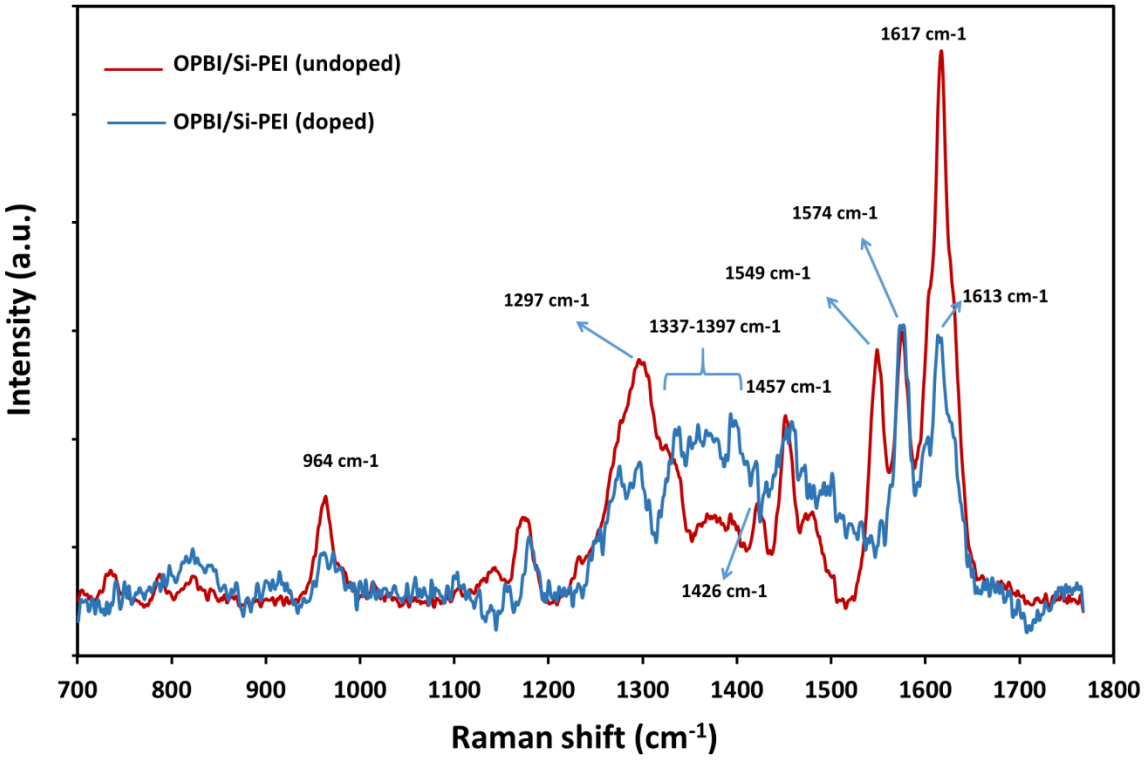

Figure 5. 11. Raman spectra of OPBI/Si-PEI undoped and doped films

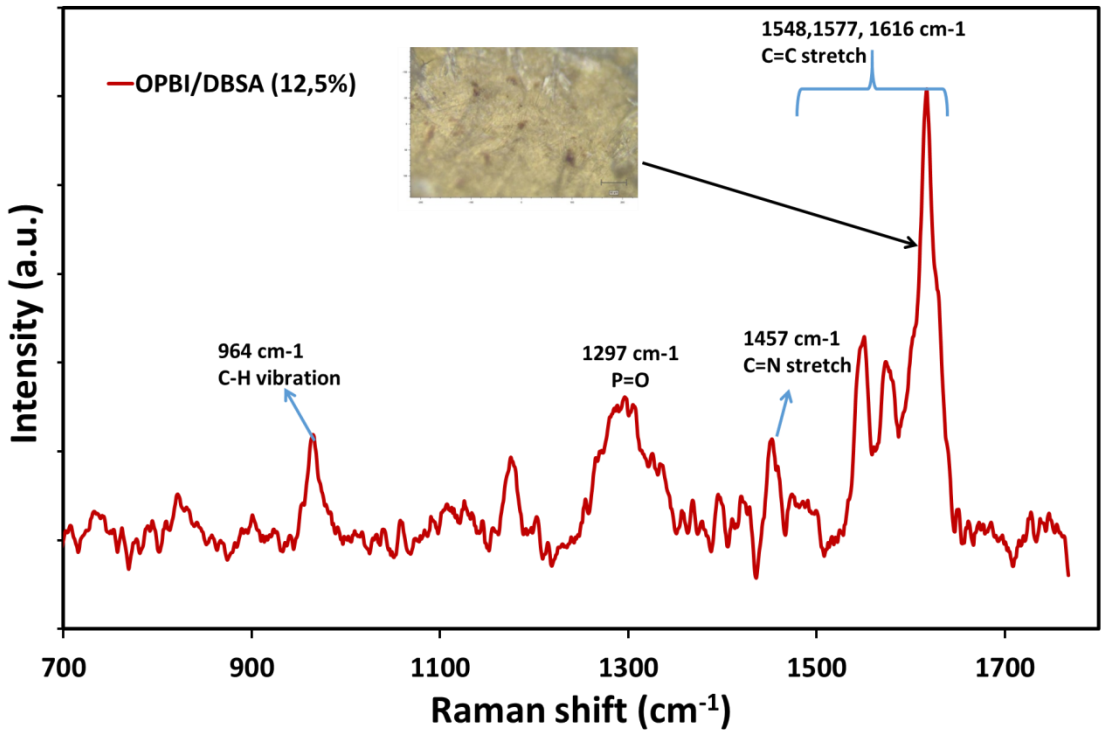

Figure 5. 12. Raman spectra of OPBI/DBSA (12,5%) undoped films

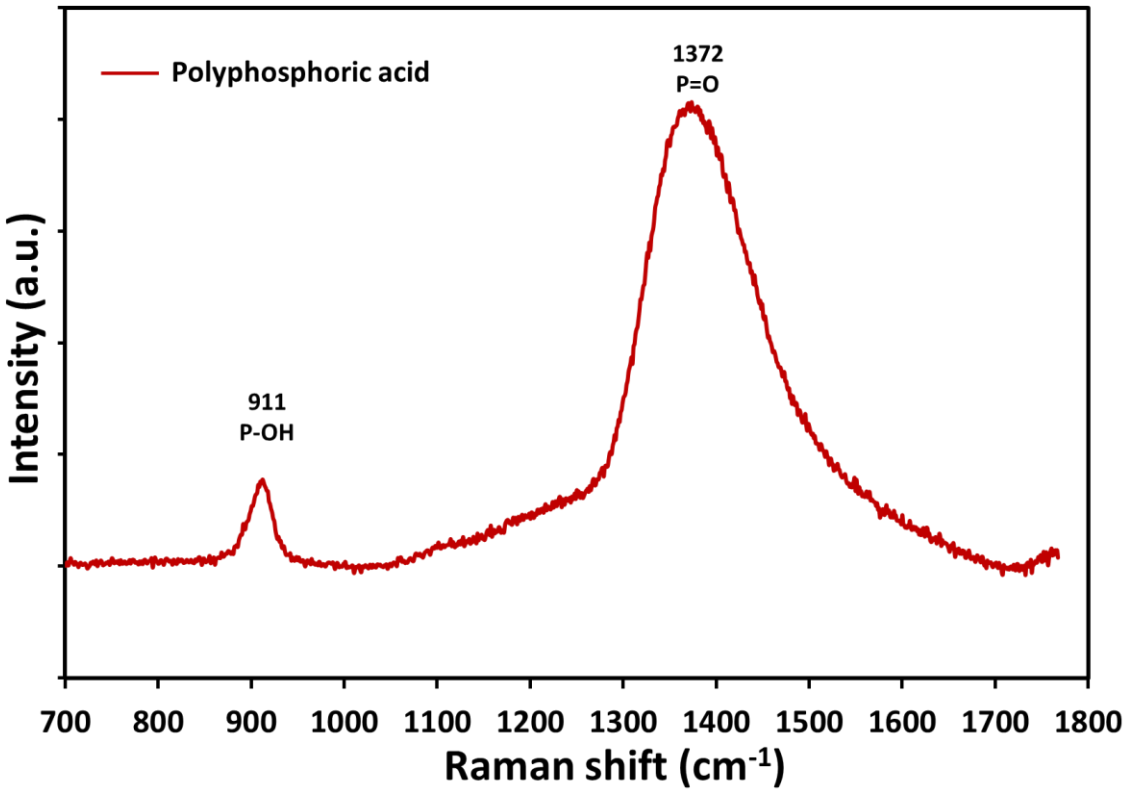

Figure 5. 13. Raman spectra of polyphosphoric acid

5.3.2. Microscopy analysis

In this section, two types of SEM tests are analysed: the morphology of the surface (topography) and the morphology of the fractured films (cross-section). With the first of the techniques what is intended to be observed is the surface of the films so that it could be able to determine if the films are homogeneous or heterogeneous, their composition, if they present precipitated particles or even if they present contaminants. With the cross-section study, the type of fracture of the films could be seen since they are previously cut with the help of liquid nitrogen (*i.e.* by cryo-fracture). Likewise, it could be determined if the surface of the membranes has the same structure as the interior.

- **Topography**

The morphology of the OPBI membranes was studied using **scanning electron microscopy** technique. SEM images are displayed in *Figures 5.14-5.16* and EDX results are shown in the *Figure 5.17*.

The surface of the OPBI membrane is shown in *Figure 5.14a* and *5.14b*. At first glance, it is necessary to emphasize that the surface is quite homogeneous since the convex hemispheres that appear in the image are located only on the surface and not inside the film. It probably arises from a fast

evaporation process, performed under high vacuum and temperature. This effect was not observed for other samples, therefore, we do not believe it belongs to the film morphology itself. On the other hand, from *Figure 5.17b* , where the EDX diagram is shown, the appearance of the expected C, O and P atoms must be pointed out due to the chemical composition of the polymer and since the phosphoric acid was used on its manufacture. When the membrane is doped (*Figure 5.14c and 5.14d*), the hemispheres disappeared given the film a flat and smooth appearance. As mention before, the doping process was performed with phosphoric acid (85%) for 7 days, reason why this time the P peak on *Figure 5.17d* appears much more intense and sharp than in the pristine OPBI. It should be pointed out that Na atoms in the EDX spectra is not expected to belong to ours samples, instead of it, it probably comes from water contamination.

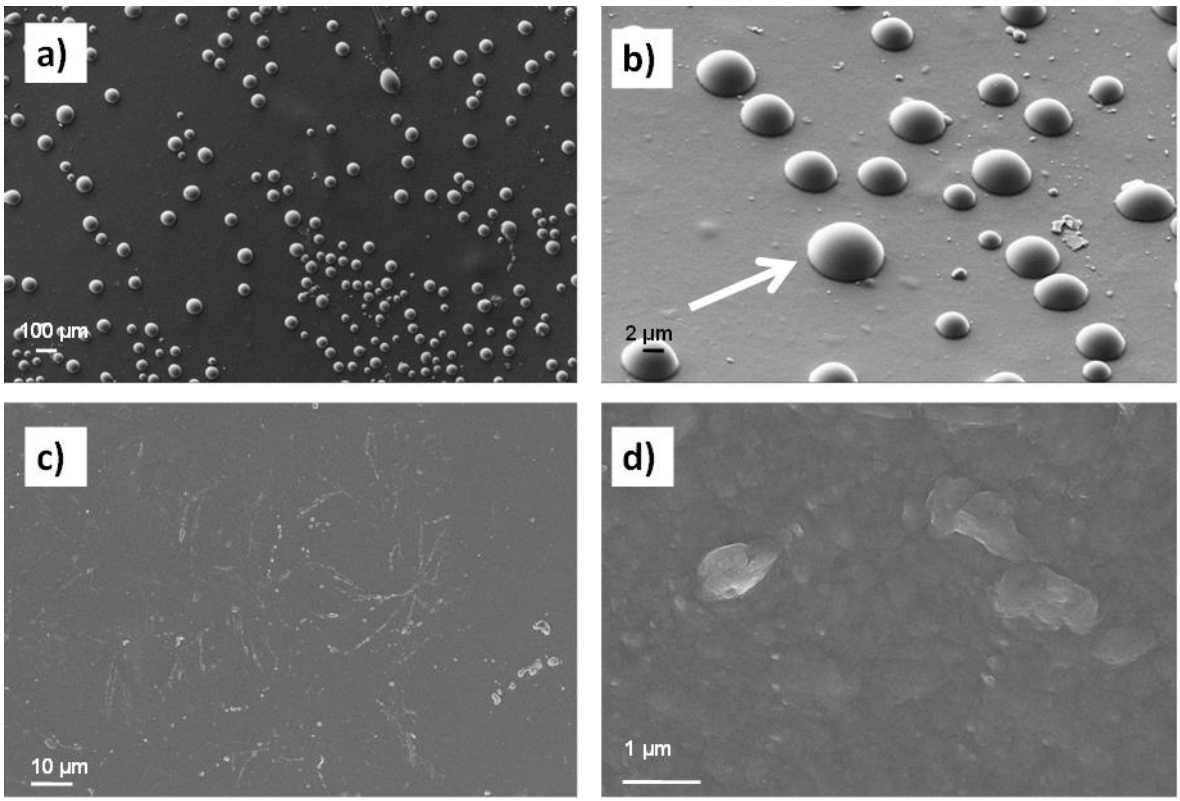

Figure 5. 14. SEM micrographs of OPBI undoped and doped: a) OPBI film (low magnification); b) OPBI film (high magnification); c) OPBI doped film (low magnification); d) OPBI doped film (high magnification). Scale bars inset.

In the case of OPBI membranes modified with silica nanoparticles (OPBI/Si-PEI), the surface of the membrane is shown in *Figures 5.15a and 5.15b*. This membrane is clearly heterogeneous since it is possible to distinguish some particles inside the films. These particles are due both to the silica and the formic acid that after drying in an oven, precipitate. It should be noted that fibre formation (*Figure 5.15b*, arrow inset) was also an indicative of the well obtaining of the polymer film. However, the strategy of functionalization of silica inorganic particles with polyethyleneimine (PEI) did not

result in a good compatibilization of Si particles inside the polymer matrix. As for the EDX diagram (*Figure 5.17f*), C and O peaks can be noted both in the white and dark parts of the film but the peak of the silica (Si) can only be detected in the white particles seen in the *Figure 5.17e*. Thus, it confirms that the silica particles had precipitated during the drying stage. After doping, once again, the film becomes more homogeneous and an intense peak of P appears in the EDX spectrum, *Figure 5.17h*.

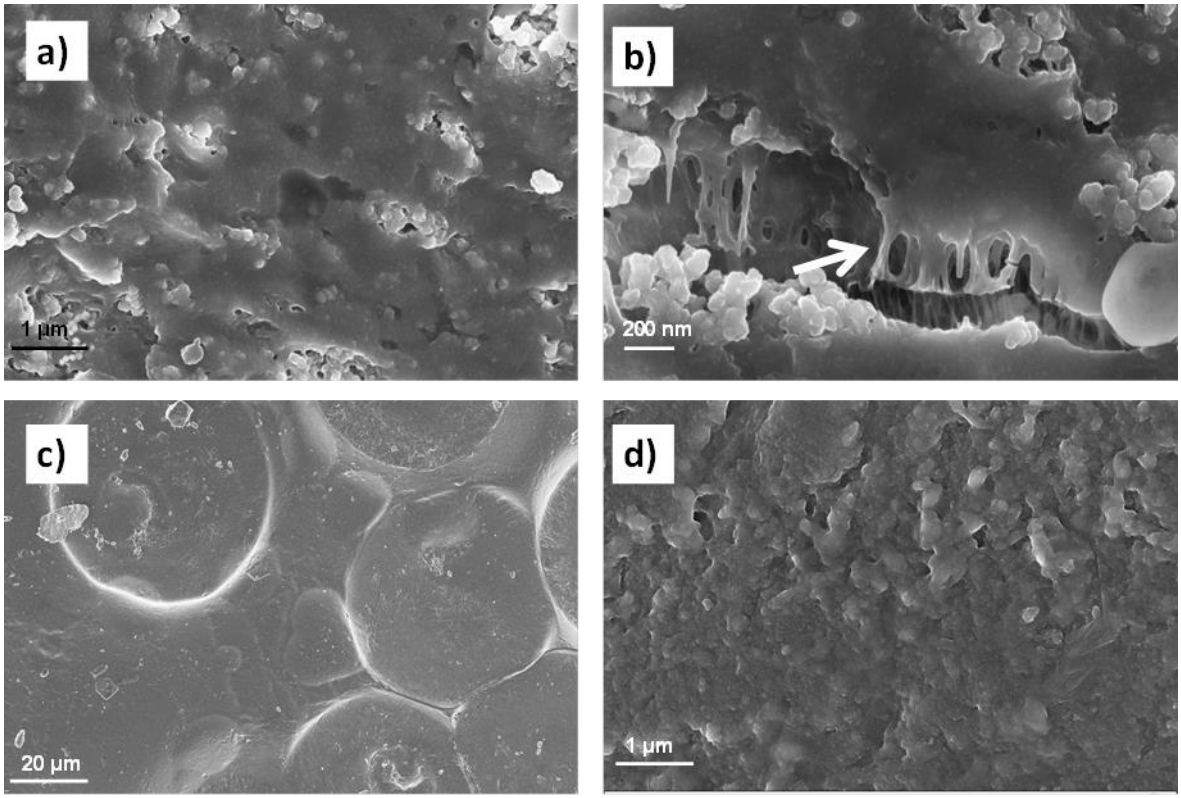

Figure 5. 15. SEM micrographs of OPBI/Si-PEI undoped and doped: a and b) OPBI/Si-PEI film (high magnification); c) OPBI/Si-PEI doped film (very low magnification); d) OPBI/Si-PEI doped film (high magnification)

Furthermore, the surface of the OPBI membrane modified with a plasticizer (OPBI/DBSA) is shown in *Figure 5.16a and 5.16b*. As the previous membranes, this one is also heterogeneous before doping and it is believed that the bright parts of the film correspond to the zones where the plasticizer was incorporated. This last statement is confirmed by the EDX chart (*Figure 5.17j*) since appears atoms appear with more intensity in that part than in the dark one. When doped, heterogeneity disappears (*Figure 5.16c and 5.16d*) and the P peak on the EDX (*Figure 5.17l*) appears reasonably, with great intensity. Therefore, SEM analysis confirms the films were well doped, in accordance to previous spectroscopy characterization results. Particularly in the case of OPBI/DBSA doped membranes, those were not possible to study by RAMAN spectroscopy.

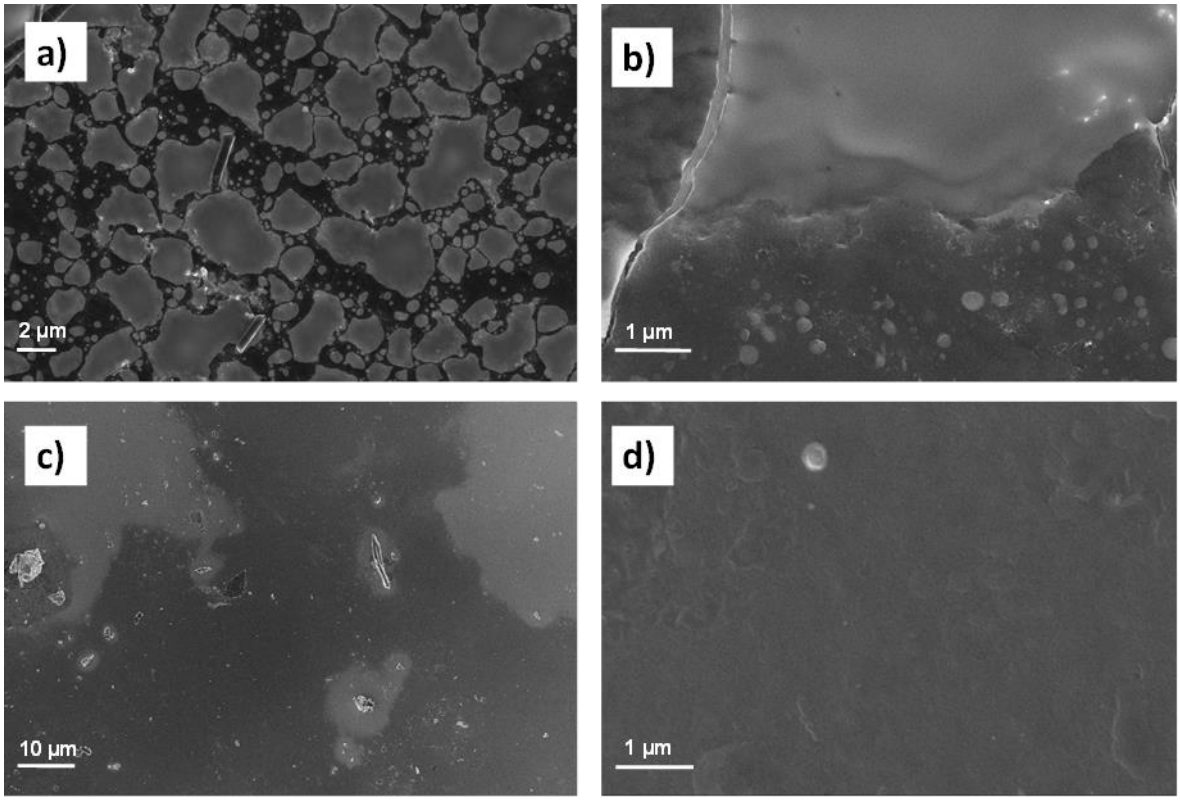

Figure 5. 16. SEM micrographs of OPBI/DBSA (5%) undoped and doped: a) OPBI/DBSA (12,5%) film (low magnification); b) OPBI/DBSA (12,5%) film (high magnification); c) OPBI/DBSA (12,5%) doped film (very low magnification); d) OPBI/DBSA (12,5%) doped film (high magnification)

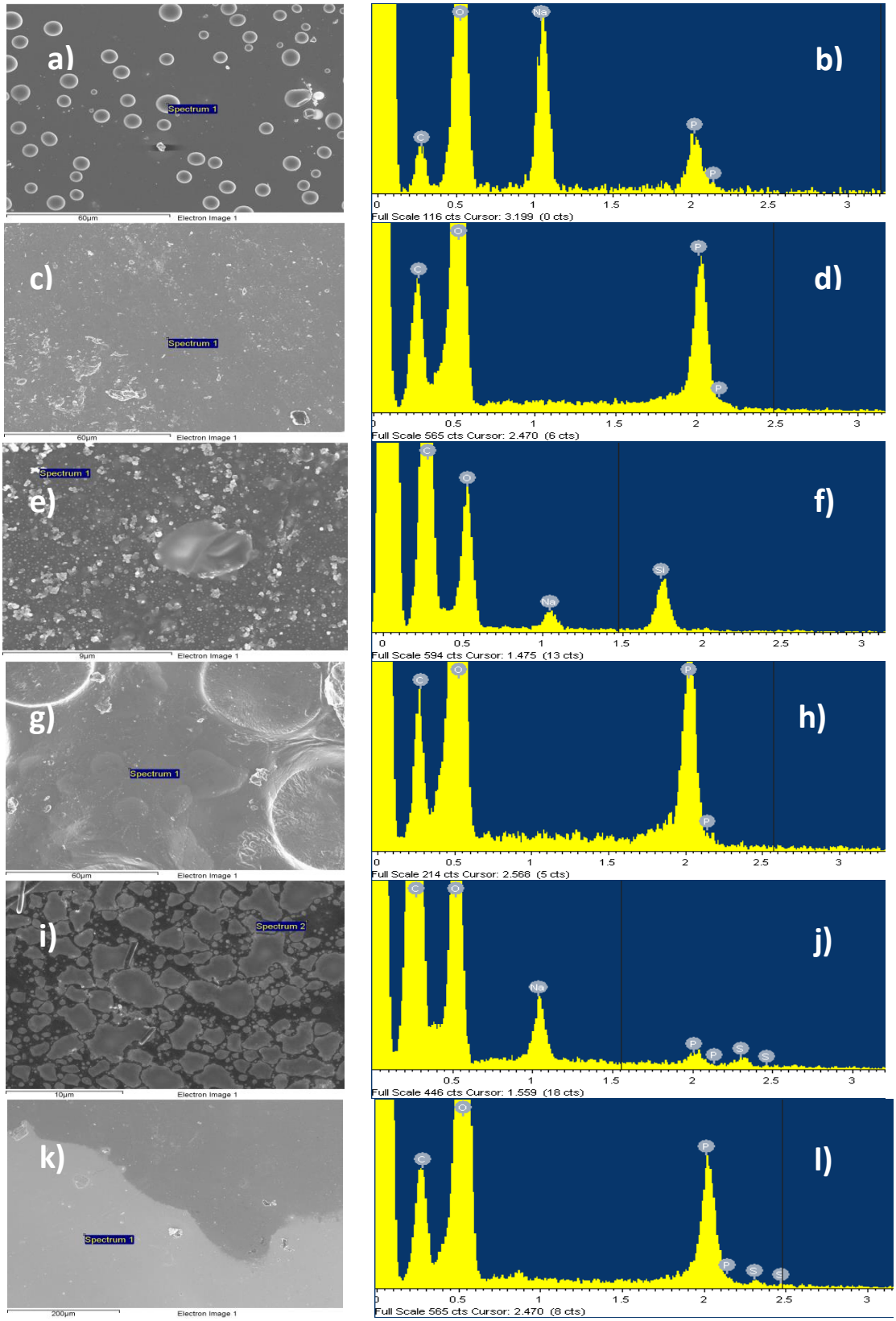

Figure 5. 17. SEM micrographs (on left) and EDX spectra (on right) of the OPBI membranes: (a-b) OPBI undoped; (c-d) OPBI doped; (e-f) OPBI/Si-PEI undoped; (g-h) OPBI/Si-PEI doped; (i-j) OPBI/DBSA undoped; (k-l) OPBI/DBSA doped.

- **Cross-section analysis**

The mechanical behaviour of the fracture was studied by analysis of the cross-section of the membranes, having been performing cryofracture with liquid nitrogen.

Figures 5.18 and *5.19*, shows SEM micrographs of the membranes' cross-section. The first set of images demonstrated the fragility of the undoped films. In *Figure 5.18b*, it can be seen internal fractures of the film that were not caused by the cryofracture treatment but were prior to it. In the image of the membrane with the plasticizer, (*Figures 5.18 c and 5.18d*), it should be noted that DBSA is in greater proportion on the surface than in the interior of the film, comparing these images with that from *Figures 5.16 a-b*. Further, this film seems to delaminate by layers unlike the previous two. Summarizing, it is possible to demonstrate that the undoped films possessed high fragility, and among the three types of membranes, the one with only 2 wt.% of Si-PEI is clearly the most fragile.

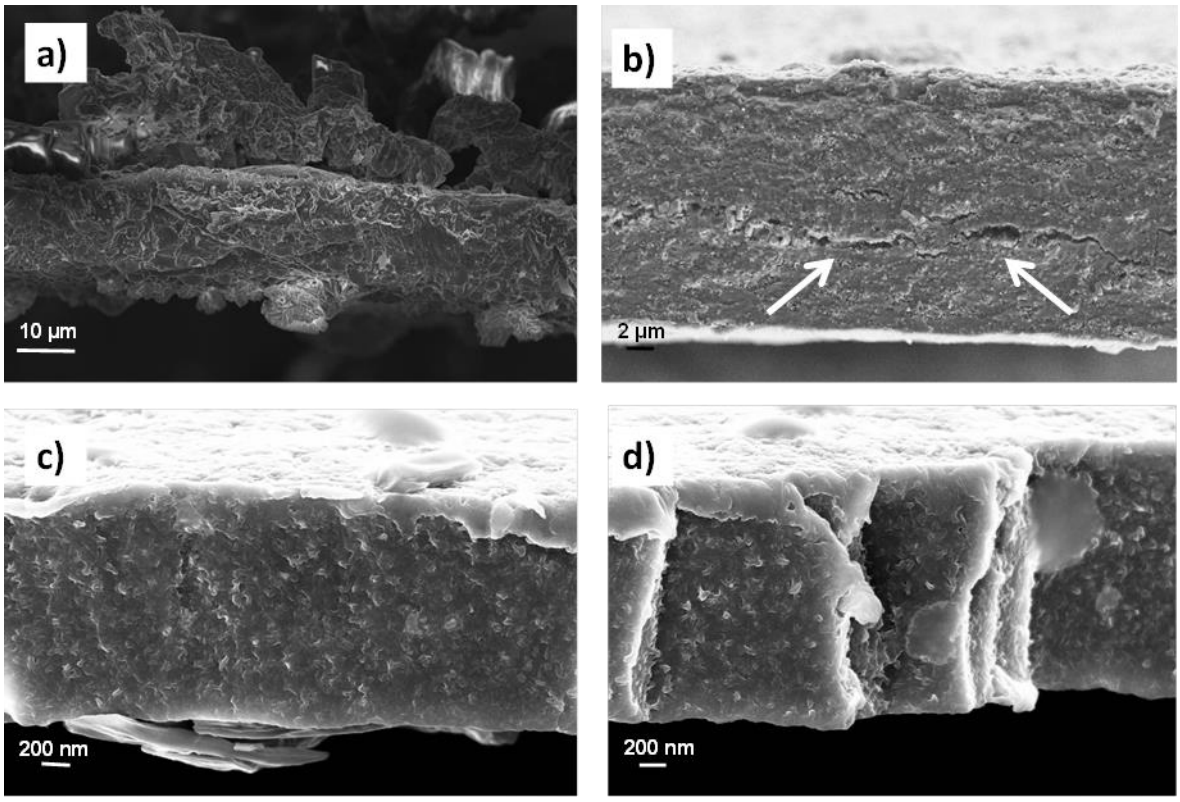

Figure 5. 18. Cross-section SEM micrographs of the undoped films: a) OPBI film (low magnification); b) OPBI/Si-PEI film (low magnification); c and d) OPBI/DBSA (12,5%) film (high magnification).

From the cross-section SEM micrographs of the doped membranes, (*Figure 5.19*), it was found that the dopant ameliorates the resilience of the films, eliminating the internal crevices that were previously observed in some of them. Thanks to the SEM images, it can be seen the growth of the cracks from the initial point of rupture, that occurs from the outer to inner surface. Beyond the

critical crack length, they grow rapidly due to the combined effects of the surface tension of the material and its internal binding forces.

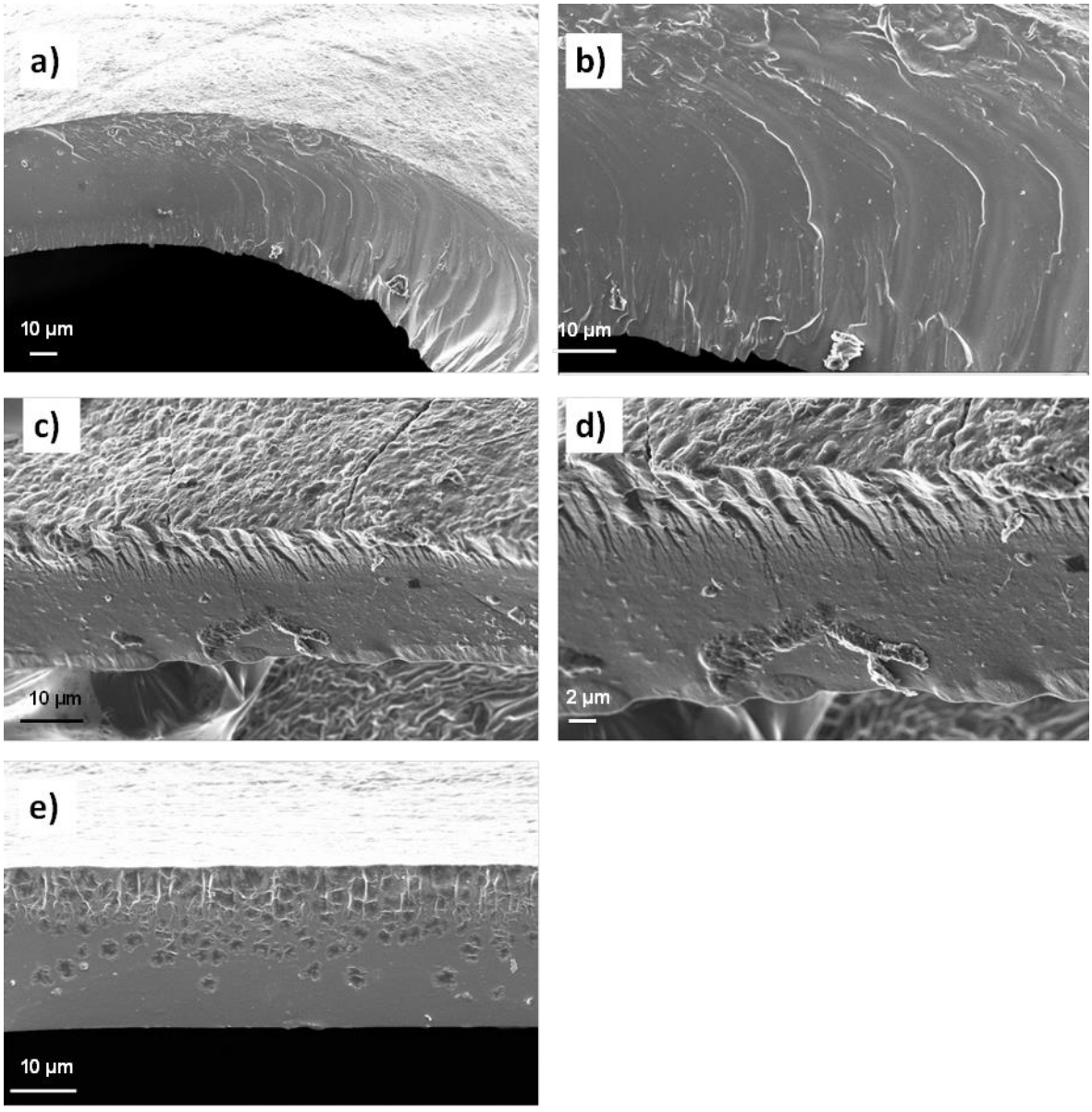

Figure 5. 19. Cross-section SEM micrographs of the doped films: a) OPBI doped film; b) OPBI doped film; c) OPBI/Si-PEI doped film; d) OPBI/Si-PEI doped film; e) OPBI/DBSA (12,5%) doped film . All them taken from low magnification scale.

5.3.3. Wettability

It has been reported that the wettability of surfaces is governed by three main parameters: the liquid-repellent properties of the compounds present at the surface, the surface morphology of topography and the roughness. (34)

The relationship between roughness and wettability was defined in 1936 by Wenzel who indicated that adding surface roughness will enhance the wettability caused by the chemistry of the surface, based on the assumption that the liquid penetrates into the roughness grooves, as in the example of *Figure 5.20*. So, if the surface is chemically hydrophobic, it will become even more hydrophobic when surface roughness is added.

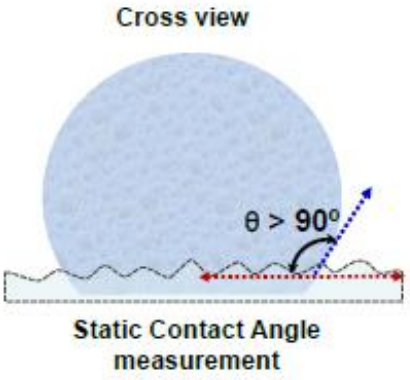

Figure 5. 20. Water contact angle on rough surface, Wenzel model (34)

As was expected, all studied films were hydrophilic displaying water contact angles (θ) lower than 90^0 due to the presence of the polar groups from the OPBI (N-H). OPBI is known by its high solubility in strong protonic acids (for instance, sulfuric acid or methanesulfonic acid) but it has also been observed its solubility in weaker acids like formic acid, and in non-acidic media.

Nevertheless, in the present study the wettability observed can be explained in basis on the roughness of the films, which increase with the presence of the inorganic and organic fillers favouring the formation of valleys and hills, as was previously observed by SEM. The image taken by the OCA 20 equipment with the membranes used in this project can be seen in the *Figure 5.21.*

The average values of the water contact angle (θ) determined for OPBI, OPBI/Si-PEI and OPBI with DBSA (doped and undoped) measured with a steel reference are shown in *Chart 5.1*.

Chart 5. 1. Values of water contact angle (θ, in degrees)

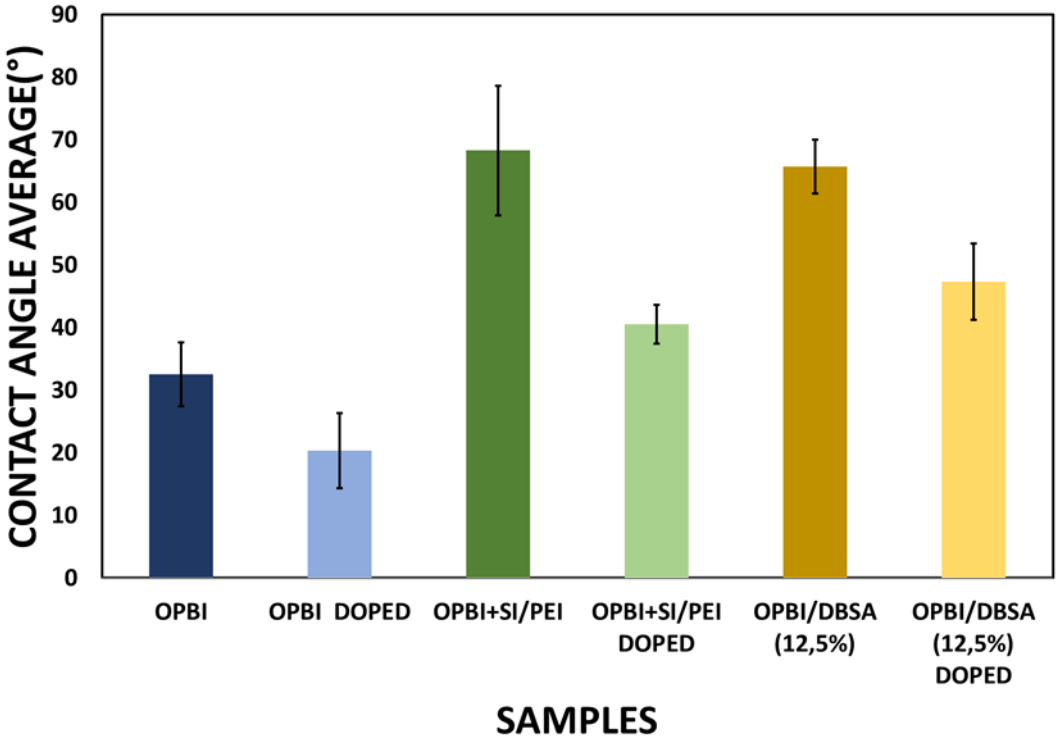

OPBI is well known by its hydrophilic properties in water and it is clear that the incorporation of both Si-PEI and DBSA intensifies its inherent hydrophilicity. It is noticeable that doping the films with phosphoric acid result in a decrease of the average contact angle by 20-30 % in every case, as expected. It should be pointed out that the WCA procedure, from the OPBI/DBSA (12,5%) doped film, had to be recorded by video with the OCA 20 equipment and the measurements were extracted from images taken from that video It was due to the very high hydrophilic behaviour obtained with this sample.

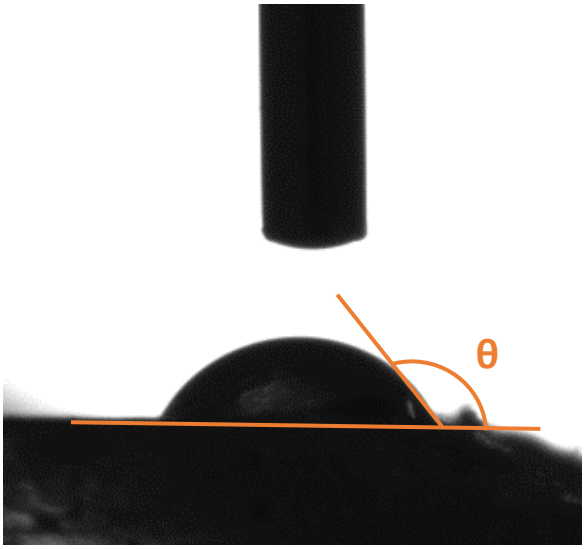

Figure 5. 21. Water contact angle on OPBI films

5.3.4. Thermal stability

As explained in the introduction section, acid doped polybenzimidazoles (PBIs)/functionalized PBIs polymer electrolyte membranes are familiarly known by their high proton conductivity with thermo-mechanical stability. TGA thermograms of OPBI, OPBI/Si-PEI and OPBI with DBSA (*Figure 5.22*) show that the polymer composites synthesized here, have very high decomposition temperatures. As can be seen, in the Figure 5.22, the first stage of weight loss occurred below 100^0C, and this could be related to the evaporation of small percentage of water molecules trapped inside the polymer matrix. The second weight loss, in the case of OPBI, from 500 to 700^0C is due to the degradation of the polymer chains. It can be seen from the figure that the thermal stability of OPBI/Si-PEI nanocomposite membranes, when compared to pristine OPBI, decreases after 200^0C. This could be due to the decomposition of the long chain amine molecules present on the silica surface that adds to the degradation of the polymer chains. In the case of OPBI with DBSA plasticizer, it is observed again that the thermal stability of the film decreases after 200^0C but differs from the other two films in the instability of the degradation, as well as in the degradation rate. It should also be emphasized that the pristine OPBI is the only one with a third degradation step at 900^0C, leading to the lowest value of char yield at 1000^0C.

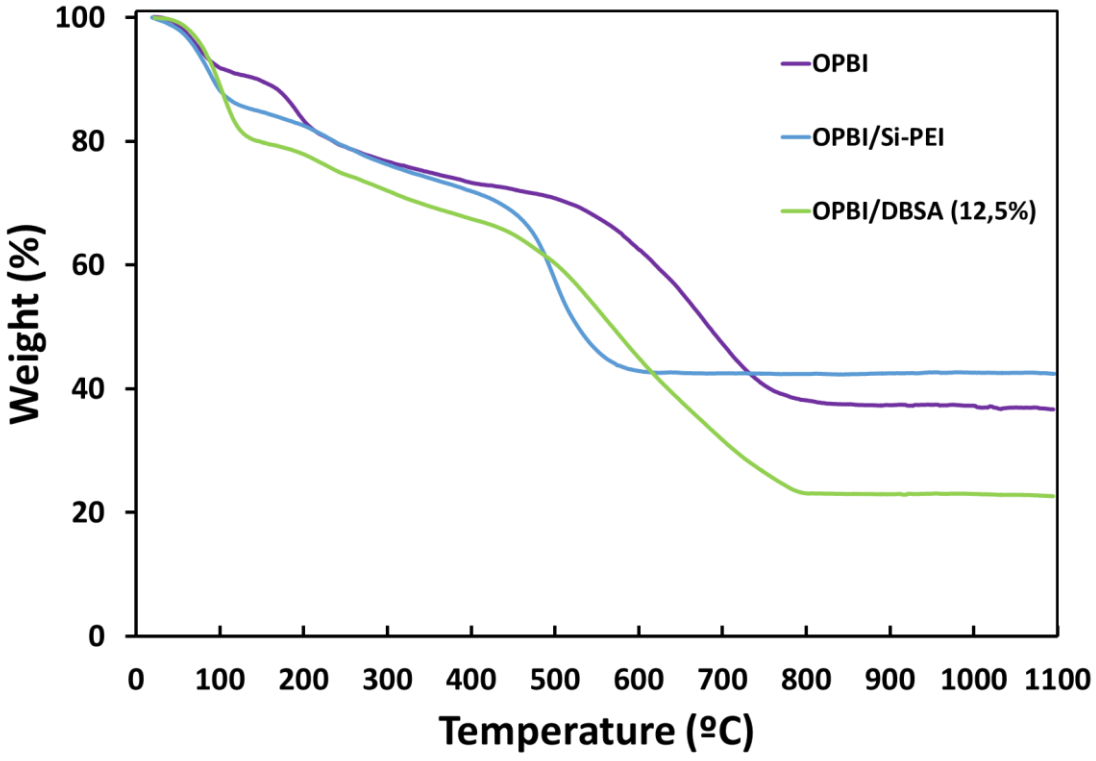

Figure 5. 22. Thermograms of pristine OPBI membranes and OPBI samples modified with Si-PEI and DBSA molecules. All them in the undoped state.

The weight loss percentage decreased from about 42% for the OPBI/Si-PEI to just about 36% for the neat OPBI, and of 22% for the OPBI with the plasticizer at 1100^{0}C, *Chart 5.2*. This might be caused by two reasons: (i) the presence of silica particles helps the decreasing the moisture absorption tendency of the polymer membranes; and (ii) the presence of both silica particles and the plasticizer make them act as thermal shields, protecting the polymer chains from being subjected to heat. As for the degradation temperatures (*Chart 5.2*), it is clear that when the degradation is about a 20% of weight, the sample that decomposes at less temperature is the one with the plasticizer (DBSA), while the other two films had more or less the same degradation temperature. Thus, it can indicates that the OPBI/DBSA composite absorbs more water than the other films, on its preparation step; despite all films were previously dried in a vacuum oven at 110^{0}C for 5 days.

However, when the decomposition reaches the 50%, the pristine OPBI film has the highest decomposition temperature, being more thermally stable than OPBI/DBSA film and OPBI/Si-PEI membranes.

Chart 5. 2. Thermogravimetric data of the films studied in this project

Sample	$T_{initial}$ (°C)	$T_{0.2}$* (°C)	$T_{0.5}$* (°C)	Char yield** (%)
OPBI	20	235	684	37
OPBI/Si-PEI	19	236	527	42
OPBI/DBSA 12,5%	22	147	568	23

**$T_{0.2}$ and $T_{0.5}$ correspond to the temperatures after 20% and 50% of degradation, respectively.*

***Char yield at 1100^{0}C.*

5.3.5. Water uptake, swelling ratio and swelling volume

It is known that OPBI is hydrophilic and has high affinity for moisture due to the tendency of –NH and acid groups to form hydrogen bonds with water molecules (16). After immersion of the membrane in distilled water for 3 days, it was found that OPBI can absorb about 9% of water with respect of the dry membrane. On the other hand, for the membranes that were doped in PA (85%), immersion must take place in this media, as well, for 5 days to prevent the doping from spoiling.

From *Chart 5.3*, we can see reduction in the swelling ratio capacity of the OPBI and OPBI/Si-PEI membranes when comparing pairs with the same composition, undoped and the ones doped, whereas the OPBI with DBSA plasticizer has the contrary effect. The presence of silica nanoparticles in the polymer matrix would prevent the motion of OPBI chains and makes them more rigid related

to the pristine OPBI films; thus preventing the separation between the stacked polymer backbones caused by the doping acid molecules.

As for the swelling volume, there is a general increase between the films that were not doped and the ones doped with PA. This means that the polymer OPBI doped in its three varieties absorbs greater quantity of liquid than its undoped counterparts do. Additionally, our results is in accordance with previous reported works, where they discussed the difficulty to measure the water uptake of the OPBI membranes as well as the OPBI/Si-PEI films. (12)(14). In fact, there is no record of these samples due to the poor stability of the doped films in water. On the other hand, when the plasticizer is used, the integrity of the film improves and that is the reason why it is more stable and we can obtain a value for the water uptake when the membrane is doped with PA. Comparing the OPBI/DBSA undoped and doped water uptake, the late film has been increased by a factor of 9 times the first.

Chart 5. 3. Water Uptake, Swelling Ratio, and Swelling Volume in water of OPBI and nanocomposite membranes.[a)]

Sample	Water uptake (%)	Swelling ratio (%)	Swelling volume (%)
OPBI	8,94 (±1,29)	19,36 (±4,08)	30,32 (±7,70)
OPBI doped	-[b)]	0,79 (±1,11)	60,71 (±23,16)
OPBI/Si-PEI	45,27 (±7,69)	6,72 (±2,90)	1,08 (±1,21)
OPBI/Si-PEI doped	-[b)]	2,03 (±1,95)	24,43 (±4,01)
OPBI/DBSA (12,5%)	3,07 (±0,70)	1,63 (±0,91)	9,41 (±1,76)
OPBI/DBSA (12,5%) doped	28,08 (±4,08)	2,20 (±2,53)	47,93 (±17,1)

[a)] The standard deviation of measurements is shown in parentheses.
[b)] The OPBI doped sample was not possible to measure due to its lack of film integrity in water medium.

Therefore, to conclude, OPBI/DBSA (12,5 wt.%) seems to have the good solvent swelling properties to be used as PBI-based fuel cell membrane. However, the conductivity data must be approached.

5.3.6. Proton conductivity measurements

Prior to the start of the proton conductivity measurements, all the membranes were dried by heating at 100^0C to avoid the effect of moisture and to prevent the cell from being oxidized by the action of phosphoric acid. The complete procedure was described on the section 4.5.6.

As stated before, OPBI membranes in doped conditions have better mechanical integrity than the undoped ones. It was also reflected in the conductivity experiments, when they had to be fitted inside the capacitor cell described on Figures 4.15-4.16.

The proton conductivity of all the composite membranes was measured in the range of 22–180^0C by using EIS spectroscopy. Accordingly, two kind of plots can be obtained: the Nyquist and the Bode plots. In this work, only the Bode curves have been compared and the proton conductivities of the OPBI and that of the OPBI composite membranes obtained from the Nyquist plots (not shown here) are reported in the *Chart 5.4*. In all the three composites, the proton conductivities and the Bode plots of the membranes were compared between doped and undoped states.

In previous works, the proton conductivity usually increases with increasing temperature(29). Although, in our case, we observed mostly drops in proton conductivity beyond 100-180^0C (*Chart 5.4*). It is probably due to the instability of the PEM at high temperature for long time (48h for stabilization). By contrary, when comparing the doped and undoped states of one unique system, it can be seen that the proton conductivity is higher for the doped films, as expected for this type of high temperature thermoplastic (*Figure 5.23*).

The values indicate that pristine OPBI doped and OPBI/DBSA doped composites had the better proton conductivities, compared to the other samples. In fact, the proton conductivities of OPBI/DBSA composites are very close to that of pristine OPBI sample, which is also the manifestation of the good stability of this composite. Thus, 12,5 wt.% of DBSA load in PEM, can help the polymer to improve its mechanical properties without decreasing the electrical properties.

On the other hand, OPBI/Si-PEI had the worse electrical behaviour due to the inhomogeneity of nanoparticles dispersion, as observed by SEM. The poor mechanical property of this film, prevent it to be measured at high temperatures. Therefore, this composition would not have an effective applicability as PEM.

Chart 5. 4. Proton conductivity of OPBI, OPBI/Si-PEI and OPBI/DBSA (12,5%) membranes

Membrane	Membrane state	Temperature (^{0}C)	Resistance (Ω)	Thickness (µm)	Width (mm)	σ (S/cm)
OPBI	undoped	22	7,41E+05	45,4	15	3,97E-05
		100	2,38E+05			1,23E-04
		180	1,49E+05			1,97E-04
	doped	22	1,99E+04	22,9	14,7	2,98E-03
		100	6,88E+03			8,64E-03
		180	4,34E+04			1,37E-03
OPBI/DBSA (12,5%)	undoped	22	3,94E+05	20,6	14,8	1,66E-04
		100	8,73E+06			7,51E-06
		180	4,21E+05			1,56E-04
	doped	22	4,84E+04	42,9	15	6,42E-04
		100	2,79E+05			1,11E-04
		180	7,12E+05			4,36E-05
OPBI/Si-PEI	undoped	22	4,52E+05	17,1	14,7	1,76E-04
		100	-	-	-	-
		180	-	-	-	-
	doped	22	7,00E+05	61,9	15	3,08E-05
		100	5,88E+06	61,9	15	3,66E-06
		180	-	-	-	-

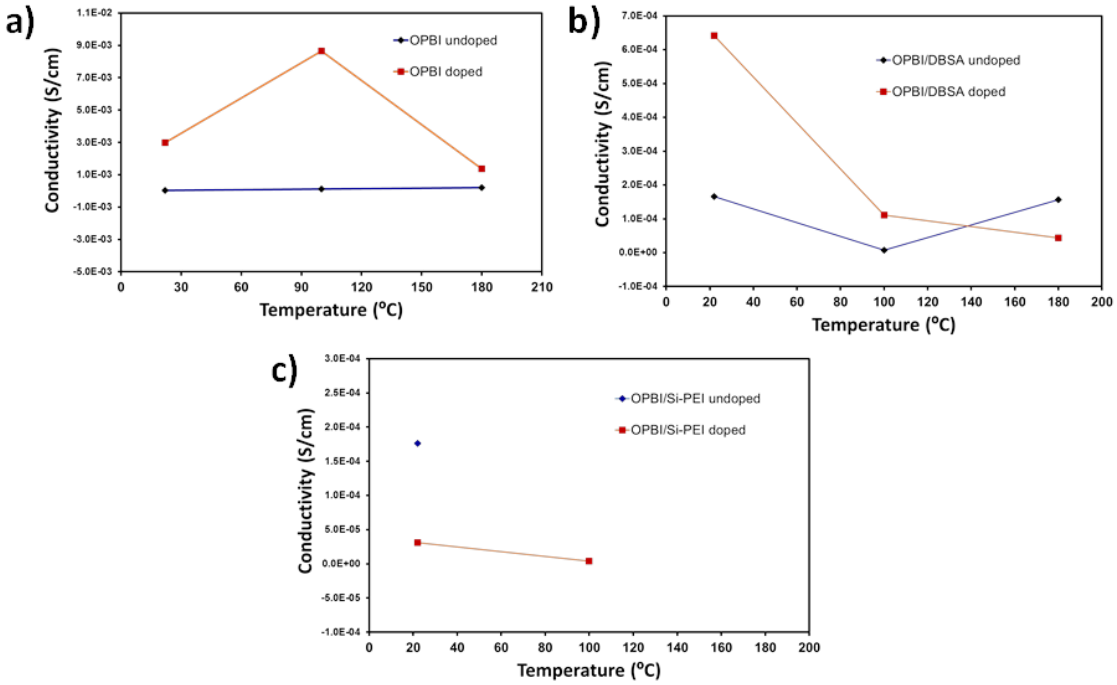

Figure 5. 23. Conductivity measurements: a) OPBI doped and undoped; b) OPBI/DBSA (12,5%) doped and undoped; c) OPBI/Si-PEI doped and undoped

The proton conductivities showed in the *Chart 5.4* were measured employing the values of the film resistance (R_2) taken from a simple electrical circuit [(R_1(R_2Q_1)]. Therefore, the data provided are not precise. For a better interpretation of these results, we will need devote time to try other electrical circuits that can adjust the experimental data. However, observing the Bode plots (*Figures 5.24-5.28*), some of our discussion is validated. The phase angle (edge Y2, on right) is an indicative parameter of the insulating or conductive properties of the film, at high frequencies. When this value is close to 90 degrees, the samples are mostly insulating, whereas if it is close to zero degree, it will be conductive. The undoped samples have phase angle starting close to 60-70 degrees and the doped samples dropped to approximately 5 degrees.

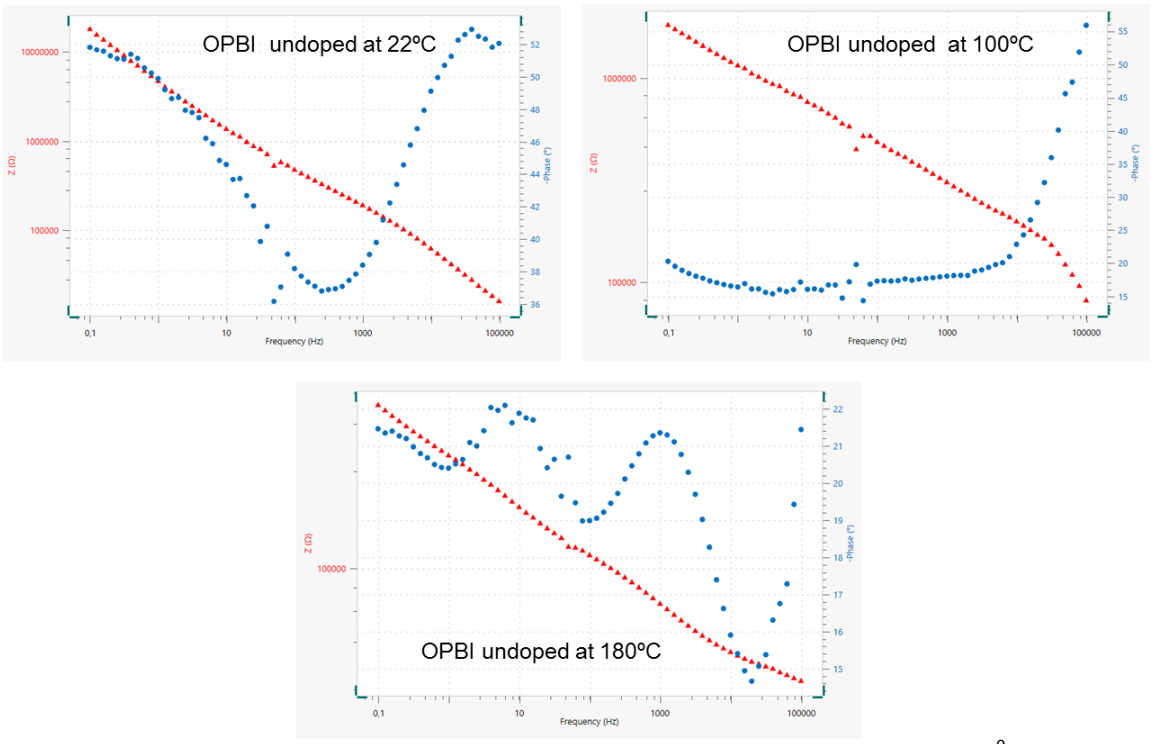

Figure 5. 24. OPBI undoped Bode curves at different temperatures (22,100 and 180^{0}C)

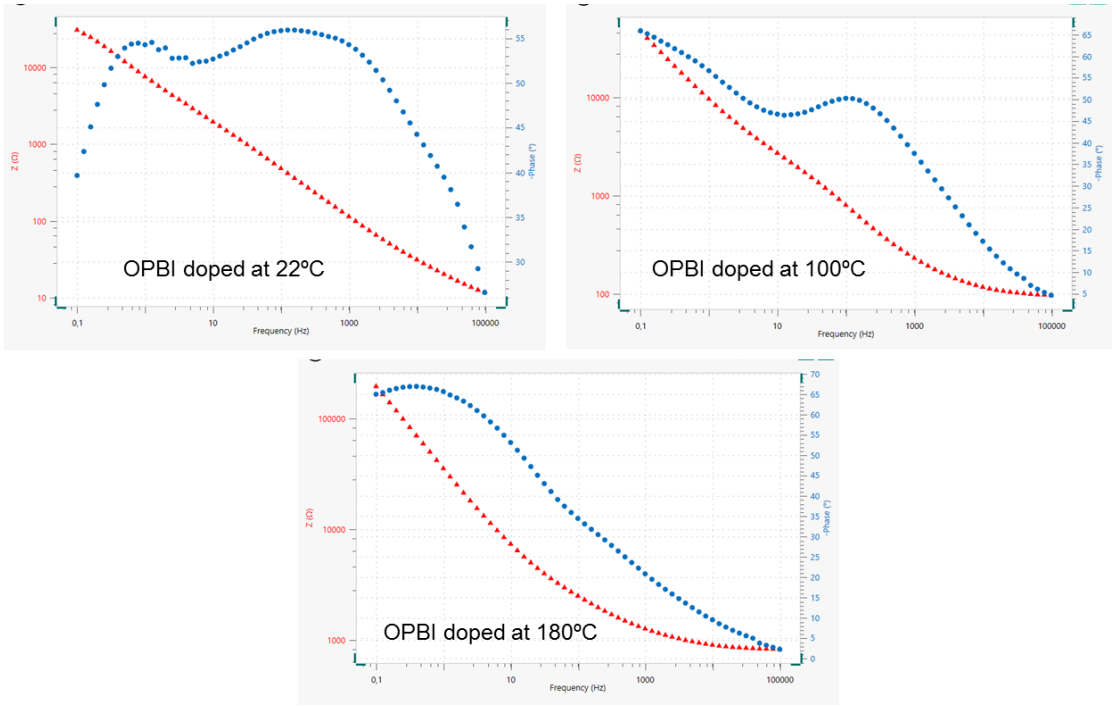

Figure 5. 25. OPBI doped Bode curves at different temperatures (22,100 and 180^{0}C)

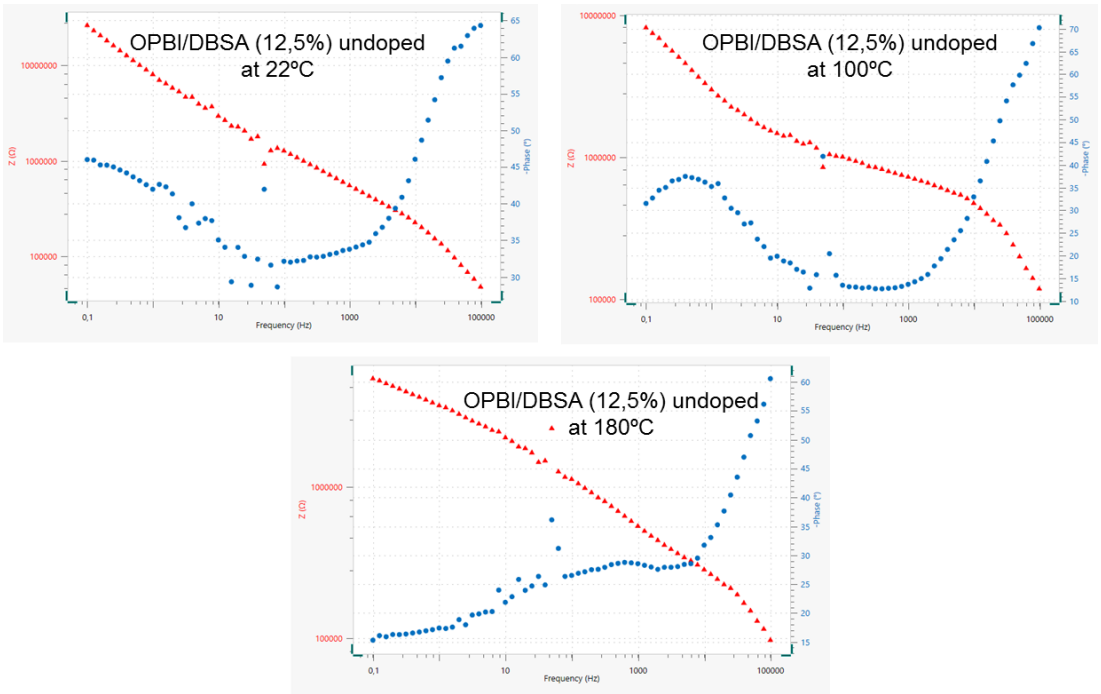

Figure 5. 26. OPBI/DBSA (12,5%) undoped Bode curves at different temperatures (22,100 and 180^{0}C)

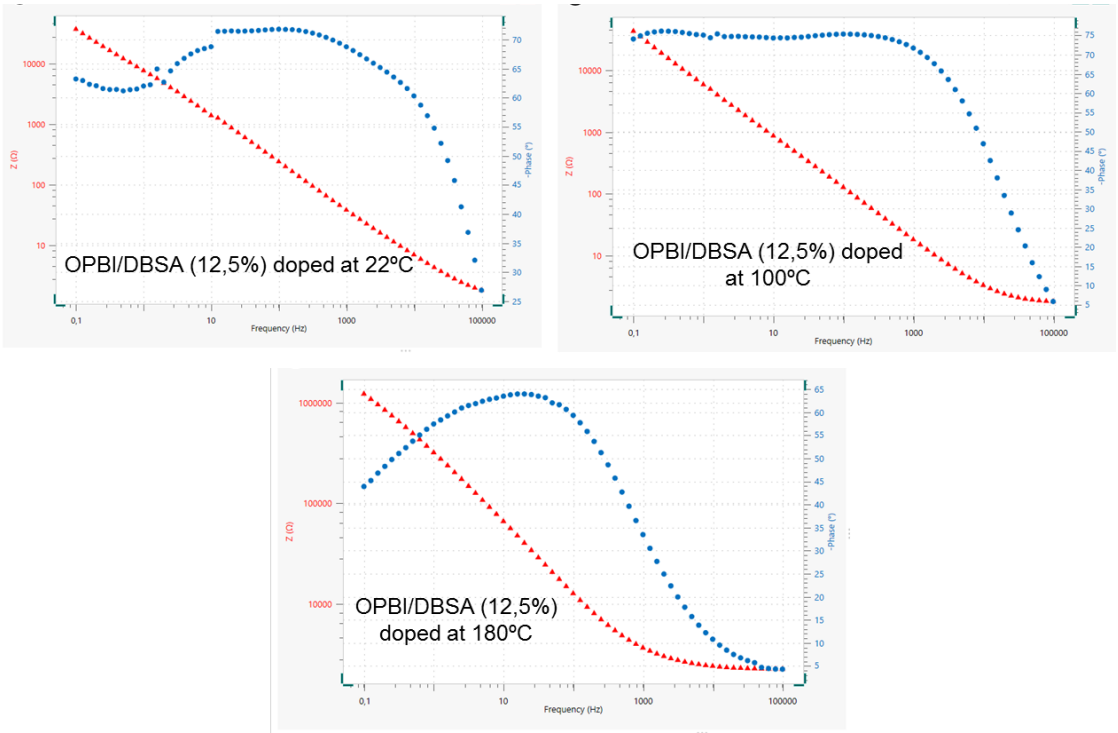

Figure 5. 27. OPBI/DBSA (12,5%) doped Bode curves at different temperatures (22,100 and 180^{0}C)

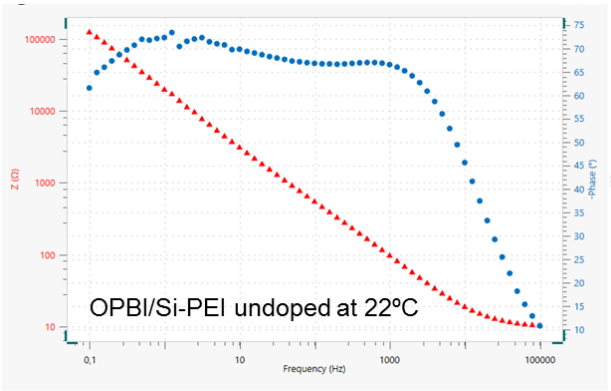

Figure 5. 28. OPBI/Si-PEI undoped Bode curves at different temperatures (22^{0}C)

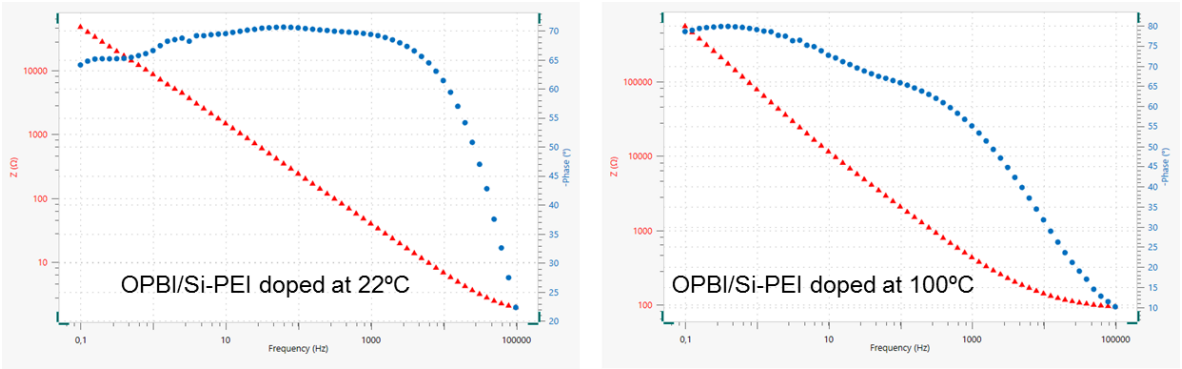

Figure 5. 29. OPBI/Si-PEI doped Bode curves at different temperatures (22 and 100^{0}C)

6. Environmental impact analysis

This section describes a study of the possible environmental impact caused by the synthesis of the OPBI films, including energy consumption, gas emissions and the elimination of waste generated during the project.

In addition, an analysis of the substance's hazards used during the realization of this project will be carried out following the European Union regulations in force. The regulation is subject to the REACH standards that encompass the regulatory framework for the management of chemical substances.

6.1. Energy consumption and emissions

An aspect to take into account in the environmental impact analysis is the generation of carbon dioxide emissions due to the consumption of electricity. This consumption comes from two main components: the drying oven, with a power of 1,4kW and the extractor hood, with a power of 0,25 kW. The electricity observatory, in its January 2016 bulletin (40) states that the annual average for 2012 is 0,146 kg of carbon dioxide per kW·h consumed. For other greenhouse gases such as nitrogen oxides (NO_x) and for sulfur dioxide (SO_2) values are 0,220 g NO_x/kW·h and 0,309 g SO_2/kW·h, respectively.

If it is considered a treatment of 400 h in the extractor hood and another 650 h in a heating stove, the total consumption results in **1010 kW·h**:

i) Extractor hood: 0,25 kW·400 h = 100 kW·h
ii) Heating stove: 1,4 kW·650 h = 910 kW·h

Therefore, the quantities of gases mentioned that are estimated to have been emitted into the atmosphere are:

i) 1010 kW·h·0,146 kg CO_2/kW·h= 147,46 ≈ 147 kg of CO_2
ii) 1010 kW·h·0,309 g SO_2/kW·h= 312,09 ≈ 312 g of SO_2
iii) 1010 kW·h·0,220 g NO_x/kW·h= 222,20 ≈ 222 g of NO_x

Therefore, this can be considered the global contribution of this project to air pollution in the city of Barcelona and the global greenhouse effect.

6.2. Environmental impact of experimental phase

To identify the impacts produce during the investigation, it is necessary to understand that the cause of the environmental impact is the activity and the consequence is the impact. This concept is shown and explained in *Figure 6.1*.

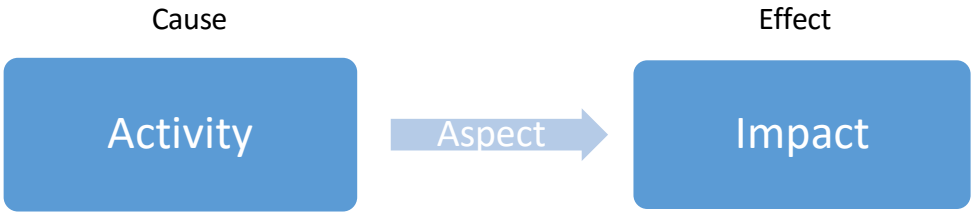

Figure 6. 1. Scheme to identify environmental impacts

In concordance with the past concept and considering as main aspect the use of chemical reagents, the principal impacts generated during experimental phase can be analysed in *Figure 6.2*. In order to prevent these effects was necessary: follow the normal lab safety rules (wear lab coats, gloves and protection glasses), store products and reagents in controlled atmospheres with proper ventilation and taking into account supplier's recommendations.

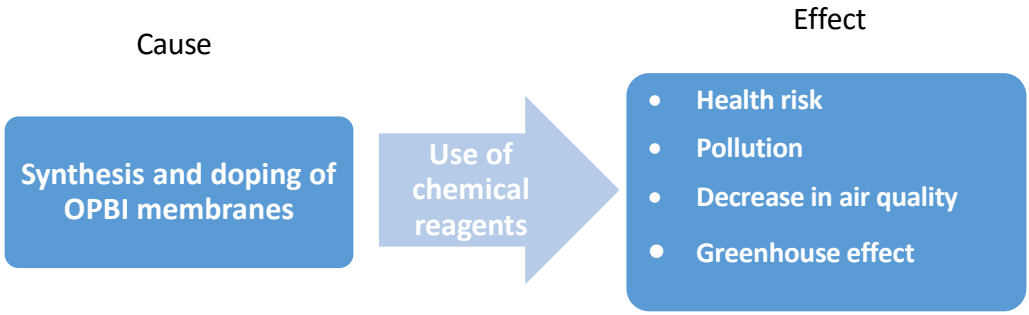

Figure 6. 2. Causes and effects produced during this investigation

6.3. Treatment of waste generated

The waste generated during the execution of this project was, mainly, non-chlorinated substances, acids and solid waste that were disposed in special containers, depending on their nature. Subsequently, a specialized external company destroys the contents of the containers according to current regulations.

6.4. Substance's hazards

Regulation (EC) Nº 1907/2006 (hereinafter referred to as REACH, acronym of Registration, Evaluation, Authorization and Restriction of chemical substances and mixtures) entered into force on June 1st 2007 and whose main objective is to improve protection for human health and the environment against the risk that the manufacture, commercialization and use of the chemical substances and mixtures can entail.(41)

REACH standard applies to all chemical substances present in daily life, either as such, in mixtures or contained in products, and is therefore applicable in economic sectors of diverse nature.

To comply with REACH provisions, companies must identify and manage the risks associated with the substances they manufacture and market in the European Union. They must demonstrate how to use these substances safely and communicate all information related to risk management measures to all parties involved.

According the current regulation, Chart 6.1 shows the substances classified as dangerous and their pictograms, whereas in the Chart 6.2 their Hazard Statements are indicated, according to the established codes.

Chart 6. 1. Classification of the dangerous substances

Chemical substance	Danger	Pictogram
Formic Acid	GHS02, GHS05, GHS06, GHS07,GHS08	

o-Phosphoric Acid	GHS05, GHS07	
3, 3', 4, 4'-tetraaminobiphenyl (TAB)	H302, H319, H341, H350	
Tetraethyl orthosilicate (TEOS)	GHS02, GHS07	
4, 4'-oxybis(benzoic acid) (OBA)	GHS07	
Dodecylbencenesulfonic acid (DBSA)	H302, H314	
N-(3-trimethoxysilylpropyl) diethylenetriamine (TMSPDT)	H315, H317, H318, H332, H412	

Chart 6. 2. Hazard Statements meaning

Hazard Statement	Meaning
GHS02	Flammable
GHS05	Corrosive
GHS06	Acute toxicity
GHS07	Health hazard
GHS08	Serious health hazard
H302	Harmful if swallowed
H314	Causes severe skin burns and eye damage
H315	Skin corrosion/irritation
H317	Skin sensitisation
H318	Serious eye damage/eye irritation
H319	Causes serious eye irritation
H332	Acute toxicity (inhalation: dust, mist)

H341	Suspected of causing genetic defects
H350	May cause cancer
H412	Hazardous to the aquatic environment

We can confirm that, in this project, all the above reagents were manipulated according to their hazard statements to avoid any skin contact, inhalation, or any injuries.

7. Conclusions

The present work looked for a methodology to obtain a conductive polymer membrane, based on the modification of OPBI polymer with the addition of Si-PEI NPs and DBSA fillers, in order to be able to use it in fuel cells applications. It is possible to obtain these membranes by direct casting on a Petri dish preceded by complete dissolution of the solute. To perform the characterization of the films, several techniques were used.

First of all, it must be highlighted the difficulty when working with OPBI films, in all varieties without doping, due to the fragility of the material (OPBI, OPBI/Si-PEI and OPBI/DBSA (12,5 wt.%). This fact held the water uptake measuring back as noted earlier. Nevertheless, it has been possible to find an adequate amount of DBSA plasticizer that greatly improves the mechanical stability of these films without doping. Regarding the mechanical stability of the doped films, it has been observed that the process of 7 days doping with phosphoric acid (85%) improves the mechanical integrity of the films and makes them more stable to immersion in the same solvent for the swelling measures.

From the FTIR and RAMAN techniques, it is possible to underscore the appearance of peaks assigned to C=C stretching from aromatic compounds, C=N stretching and C-H vibration of benzene ring, as expected knowing its structure. In addition, in the doped films appear new and broad absorption bands that clearly correspond to the phosphoric acid, which proves the acid is trapped inside the OPBI films.

From SEM micrographs, it was demonstrated the brittle properties of the undoped films, as well as the heterogeneity of these samples, when Si-PEI nanoparticles were added. From these results it can also be emphasized that the doping process is necessary for a good conductivity across the film, improves the mechanical stability and, moreover, allows to obtain more homogeneous films. In relation to these analyses, EDX tests were also performed with results close to expected. In the EDX diagrams, C, O and P atoms appear due to the chemical composition of the polymer and since the phosphoric acid was used in the manufacture of OPBI powder. When the analysis is performed on the doped films, a higher intense peak from P atoms appears in the spectra of all samples.

In the present study, wettability was studied by measuring the contact angles with water. As was expected, all the films were hydrophilic, which means that the WCAs are lower than 90^0 due to the presence of the polar groups from the OPBI (N-H, P-OH). Moreover, the addition of inorganic and organic fillers increases the roughness of the films, favouring the formation of irregularities on the surface of the membrane, which made the analysis difficult at some point. Those irregularities were also observed during the SEM topography analysis.

Thermogravimetric analysis of OPBI, OPBI/Si-PEI and OPBI with DBSA show that the polymer composites synthesized, have very high decomposition temperatures close to 400 ºC.

Finally, the proton conductivities measured by EIS, demonstrated this kind of thermoplastic has better electrical properties when they are doped, either with an inorganic or organic acid (PA or DBSA). However, their temperature stability is still disappointing.

For future works, some organic acids would be investigated (like camphorsulfonic acid or p-toluenesulfonic acid), to find a more compatible dopant acid for this type of high temperature thermoplastic. On the other hand, for the results publication, we will need explore other equivalent electrical circuits (EEC) in the EIS analysis, in order to get a more precise fitting between the experimental and the theoretical data.

8. Economic analysis

The economic evaluation of the project is presented in this section. The total budget is based on the cost of reagents employed, the personnel in charge of the study and the rent of the equipment.

8.1. Reagents cost

The cost of each reagent used during the experimental phase is displayed in Chart 8.1. In order to obtain the real cost of each reagent was necessary calculate the percentage of use.

Chart 8. 1. Final cost of each reagent

Reagents cost			
Chemical substance	**Price**	**Percentage of use**	**Cost (€)**
Formic Acid	43,50 €/L	30%	13,05
o-Phosphoric Acid	78,0 €/L	40%	31,2
3, 3', 4, 4'-tetraaminobiphenyl (TAB)	113 €/10g	25%	28,25
Tetraethyl orthosilicate (TEOS)	67,30 €/L	10%	6,73
4, 4'-oxybis(benzoic acid) (OBA)	145 €/100g	5%	7,25
Dodecylbenzenesulfonic acid (DBSA)	56,60 €/500g	3%	1,70
N-(3-trimethoxysilylpropyl) diethylenetriamine (TMSPDT)	60,60 €/100mL	30%	18,18
		TOTAL (€)	**106,36**

8.2. Equipment cost

The costs per hour of the equipment needed to perform the characterization are shown in *Chart 8.2*. (42)

Chart 8. 2. Cost per hour of the equipment used in this project

Equipment	Time (h)	Cost (€/h)	Final Cost (€)
Potenciostate-galvanostat	12,0	35,0	420
FT-IR spectrophotometer	6,0	22,50	135
Scanning electron microscope	4,5	187,50	843,75
Contact angle meter	5,0	15,0	75
RAMAN Spectroscopy	7,0	56,25	393,75
Thermogravimetric analyser	15,0	12,0	180,0
Particle Size Analizer (Laser Diffraction)	3	60,0	180
		TOTAL (€)	2.227,5

8.3. Personnel cost

The labour cost was established based on the hours spent on the project and considering a minimum salary of 8 €/h (43), marked by the UPC practices agreement. *Chart 8.3* shows the time inverted in the project and the final cost.

Chart 8. 3. Associated cost of the hours invested in the project

Activity	Time (h)	Cost (€/h)	Final cost (€)
Bibliographic research	70	8	560
Experimental test	650	8	5.200
Result analysis	190	8	1.520
		TOTAL (€)	7.280

8.4. Total cost

In general expenses were included electricity, water, basic laboratory and office material. To calculate this value, it is estimated the 10% of the past expenses. As for the consumables, the cost includes laboratory material such as petri dishes, beakers, weight paper… Thus the global cost of the project was 11.235,24 €, the final sum is shown in Chart 8.4.

Chart 8. 4. Global cost

Expense	Final cost (€)
Reagents	106,36
Consumables	600
Equipment	2.227,5
Personnel	7.280
General expenses	1.021,38
TOTAL (€)	**11.235,24**

References

1. Lee, K.-S. et al. Synthesis and Characterization of Highly Fluorinated Cross-linked Aromatic Polyethers for Polymer Electrolytes. A: *Chemistry of Materials* [en línia]. 2010, Vol. 22, núm. 19, p. 5511. Disponible a: https://doi.org/10.1021/cm101405h.

2. Huang, Y. et al. Niobium phosphates as an intermediate temperature proton conducting electrolyte for fuel cells. A: *Journal of Materials Chemistry* [en línia]. 2012, Vol. 22, núm. 42, p. 22456. Disponible a: http://dx.doi.org/10.1039/C2JM34704K.

3. Nawn, G. et al. Nanocomposite Membranes based on Polybenzimidazole and ZrO2 for High-Temperature Proton Exchange Membrane Fuel Cells. A: *ChemSusChem*. 2015, Vol. 8, núm. 8, p. 1381-1393. ISSN 1864564X. DOI 10.1002/cssc.201403049.

4. Samms, S.R., Wasmus, S. i Savinell, R.F. Thermal Stability of Proton Conducting Acid Doped Polybenzimidazole in Simulated Fuel Cell Environments. A: *Journal of The Electrochemical Society* [en línia]. 1996, Vol. 143, núm. 4, p. 1225. Disponible a: http://jes.ecsdl.org/content/143/4/1225.abstract.

5. Müller, F. et al. New sulfonated polystyrene and styrene-ethylene/butylene-styrene block copolymers for applications in electrodialysis. A: *Journal of Physical Chemistry B*. 2012, Vol. 116, núm. 38, p. 11767-11779. ISSN 15205207. DOI 10.1021/jp3068415.

6. Müller, F. et al. Measuring the Proton Conductivity of Ion-Exchange Membranes Using Electrochemical Impedance Spectroscopy and Through-Plane Cell. A: *The Journal of Physical Chemistry B* [en línia]. 2014, Vol. 118, núm. 4, p. 1102-1112. ISSN 1520-6106. DOI 10.1021/jp409675z. Disponible a: http://pubs.acs.org/doi/abs/10.1021/jp409675z.

7. FUEL CELL TODAY. «The Fuel Cell Industry Review 2012». A: *Platinum Metals Review* [en línia]. 2012, Vol. 56, núm. 4, p. 272-273. ISSN 00321400. DOI 10.1595/147106712X657535. Disponible a: http://openurl.ingenta.com/content/xref?genre=article&issn=0032-1400&volume=56&issue=4&spage=272.

8. Sannigraphi, A. et al. How the Monomer Concentration of Polymerization Influences Various Properties of Polybenzimidazole: A Case Study with Poly(4,4'-diphenylether-5,5'-bibenzimidazole). A: *Journal of Applied Polymer Science*. 2008, Vol. 111, p. 2194-2203. ISSN 09673911. DOI 10.1002/app.

9. Haque, M.A. et al. Acid doped polybenzimidazoles based membrane electrode assembly for high temperature proton exchange membrane fuel cell: A review. A: *International Journal of Hydrogen Energy* [en línia]. Elsevier Ltd, 2017, Vol. 42, núm. 14, p. 9156-9179. ISSN 03603199. DOI 10.1016/j.ijhydene.2016.03.086. Disponible a: http://dx.doi.org/10.1016/j.ijhydene.2016.03.086.

10. BZ, X. and Savadogo, O. The effect of acid doping on the conductivity of polybenzimidazole (PBI). A: *Journal of New Materials for Electrochemical Systems*. 1999, Vol. 2, p. 95.

11. Subianto, S. Recent advances in polybenzimidazole/phosphoric acid membranes for high-temperature fuel cells. A: *Polymer International*. 2014, Vol. 63, núm. 7, p. 1134-1144. ISSN 10970126. DOI 10.1002/pi.4708.

12. Singha, S. i Jana, T. Structure and Properties of Polybenzimidazole/Silica Nanocomposite Electrolyte Membrane: In fl uence of Organic/Inorganic Interface. A: . 2014,

13. Ellis, B. i Smith, R. *Polymers: A Property Database, Second Edition* [en línia]. 2, ilustra. CRC Press, 2008. ISBN 9781420005707. Disponible a: https://books.google.es/books?id=S-TKBQAAQBAJ.

14. Li, Q. et al. Water uptake and acid doping of polybenzimidazoles as electrolyte membranes for fuel cells. A: *Solid State Ionics*. 2004, Vol. 168, núm. 1-2, p. 177-185. ISSN 01672738. DOI 10.1016/j.ssi.2004.02.013.

15. Wang, K.Y., Chung, T.S. i Qin, J.J. Polybenzimidazole (PBI) nanofiltration hollow fiber membranes applied in forward osmosis process. A: *Journal of Membrane Science*. 2007, Vol. 300, núm. 1-2, p. 6-12. ISSN 03767388. DOI 10.1016/j.memsci.2007.05.035.

16. Singha, S. and Jana, T. Structure and properties of polybenzimidazole / silica nanocomposite electrolyte membrane : Influence of organic / inorganic interface. A: . p. 1-4.

17. Peighambardoust, S.J., Rowshanzamir, S. i Amjadi, M. *Review of the proton exchange membranes for fuel cell applications* [en línia]. Elsevier Ltd, 2010. ISBN 2177491223. DOI 10.1016/j.ijhydene.2010.05.017. Disponible a: http://dx.doi.org/10.1016/j.ijhydene.2010.05.017.

18. Li, Q. et al. High temperature proton exchange membranes based on polybenzimidazoles for fuel cells. A: *Progress in Polymer Science (Oxford)*. 2009, Vol. 34, núm. 5, p. 449-477. ISSN 00796700. DOI 10.1016/j.progpolymsci.2008.12.003.

19. Perry, K.A., Eisman, G.A. i Benicewicz, B.C. Electrochemical hydrogen pumping using a high-temperature polybenzimidazole (PBI) membrane. A: *Journal of Power Sources*. 2008, Vol. 177, núm. 2, p. 478-484. ISSN 03787753. DOI 10.1016/j.jpowsour.2007.11.059.

20. Li, X., Chen, X. and Benicewicz, B.C. Synthesis and properties of phenylindane-containing polybenzimidazole (PBI) for high-temperature polymer electrolyte membrane fuel cells (PEMFCs). A: *Journal of Power Sources* [en línia]. 2013, Vol. 243. Disponible a: https://doi.org/10.1016/j.jpowsour.2013.06.033%0AUR.

21. Nasef, M.M. et al. Enhancement of performance of pyridine modified polybenzimidazole fuel cell membranes using zirconium oxide nanoclusters and optimized phosphoric acid doping level. A: *International Journal of Hydrogen Energy* [en línia]. Elsevier Ltd, 2016, Vol. 41, núm. 16, p. 6842-6854. ISSN 03603199. DOI 10.1016/j.ijhydene.2016.03.022. Disponible a: http://dx.doi.org/10.1016/j.ijhydene.2016.03.022.

22. Devrim, Y., Devrim, H. i Eroglu, I. Polybenzimidazole/SiO2hybrid membranes for high temperature proton exchange membrane fuel cells. A: *International Journal of Hydrogen Energy*. 2016, Vol. 41, núm. 23, p. 10044-10052. ISSN 03603199. DOI 10.1016/j.ijhydene.2016.02.043.

23. Chuang, S.W., Hsu, S.L.C. i Liu, Y.H. Synthesis and properties of fluorine-containing polybenzimidazole/silica nanocomposite membranes for proton exchange membrane fuel cells. A: *Journal of Membrane Science*. 2007, Vol. 305, núm. 1-2, p. 353-363. ISSN 03767388. DOI 10.1016/j.memsci.2007.08.033.

24. Pu, H. et al. Organic/inorganic composite membranes based on polybenzimidazole and nano-

SiO2. A: *Electrochimica Acta*. 2009, Vol. 54, núm. 28, p. 7536-7541. ISSN 00134686. DOI 10.1016/j.electacta.2009.08.011.

25. Ghosh, S. et al. Role of Clays Structures on the Polybenzimidazole Nanocomposites: Potential Membranes for the Use in Polymer Electrolyte Membrane Fuel Cell. A: *The Journal of Physical Chemistry C* [en línia]. 2011, Vol. 115, núm. 23, p. 11474. Disponible a: https://doi.org/10.1021/jp202672s.

26. Ghosh, S., Maity, S. i Jana, T. Polybenzimidazole/silica nanocomposites: Organic-inorganic hybrid membranes for PEM fuel cell. A: *Journal of Materials Chemistry* [en línia]. 2011, Vol. 21, núm. 38, p. 14897. ISSN 0959-9428. DOI 10.1039/c1jm12169c. Disponible a: http://xlink.rsc.org/?DOI=c1jm12169c.

27. Fang, J. et al. Preparation and characterization of novel pyridine-containing polybenzimidazole membrane for high temperature proton exchange membrane fuel cells. A: *Journal of Membrane Science*. 2016, Vol. 502, p. 29-36. ISSN 18733123. DOI 10.1016/j.memsci.2015.12.006.

28. Wang, J.T.W. i Hsu, S.L.C. Enhanced high-temperature polymer electrolyte membrane for fuel cells based on polybenzimidazole and ionic liquids. A: *Electrochimica Acta*. Elsevier Ltd, 2011, Vol. 56, núm. 7, p. 2842-2846. ISSN 00134686. DOI 10.1016/j.electacta.2010.12.069.

29. Sana, B. i Jana, T. Polybenzimidazole composite with acidic surfactant like molecules: A unique approach to develop PEM for fuel cell. A: *European Polymer Journal* [en línia]. Elsevier Ltd, 2016, Vol. 84, p. 421-434. ISSN 00143057. DOI 10.1016/j.eurpolymj.2016.09.051. Disponible a: http://dx.doi.org/10.1016/j.eurpolymj.2016.09.051.

30. Chakraborty, D.S. Instrumentation of ftir and its herbal applications. A: *World Journal of Pharmacy and Pharmacutical Sciences*. 2016, Vol. 5, núm. 3, p. 498-505.

31. Cubells Pérez, M. Análisis De Pigmentos Con Espectroscopía Raman: Determinación Teórico-Experimental De La Temperatura Inducida Por El Láser. A: . 2013,

32. Piella Bagaria, J. PROTEIN-NANOPARTICLE CONSTRUCTS FOR INTRACELLULAR DELIVERY. A: . 2011, núm. February.

33. Goldstein, J. *Scanning Electron Microscopy and X-Ray Microanalysis: A Text for Biologists, Materials Scientists, and Geologists*. New York, NY: Springer Science & Business Media, 2012.

34. Armelin Diggroc, E. i Molina, B.G. Graft copolymers with a random distribution of pyrrole monomer with hydrophilic functionalities. A: . 2016,

35. Coats, A.W. i Redfern, J.P. Thermogravimetric analysis. A review. A: *Analyst* [en línia]. 1963, Vol. 88, núm. 1053, p. 906-924. Disponible a: http://dx.doi.org/10.1039/AN9638800906.

36. Espejo Miralles, Z. Investigation of Lab-on-Spoon Low-Power Realization for Smart Kitchen and AAL Scenarios. A: . 2013, p. 1-125.

37. Stöber, W., Fink, A. i Bohn, E. Controlled growth of monodisperse silica spheres in the micron size range. A: *Journal of Colloid and Interface Science* [en línia]. 1968, Vol. 26, núm. 1, p. 62. Disponible a: http://www.sciencedirect.com/science/article/pii/0021979768902725%0AER.

38. Beganskiene, A. et al. FTIR, TEM and NMR Iinvestigations of Stöber Silica Nanoparticles. A: *Materials Science (Medžiagotyra)* [en línia]. 2004, Vol. 10, núm. 9, p. 287-290. ISSN 00223093. DOI 10.1016/j.jnoncrysol.2012.11.006. Disponible a: http://internet.ktu.lt/lt/mokslas/zurnalai/medz/pdf/medz0-79/02 Beganskiene 287-290.pdf.

39. Feifel, S.C. i Lisdat, F. Silica nanoparticles for the layer-by-layer assembly of fully electro-active cytochrome c multilayers. A: *Journal of Nanobiotechnology*. BioMed Central Ltd, 2011, Vol. 9, núm. 1, p. 59. ISSN 1477-3155. DOI 10.1186/1477-3155-9-59.

40. WWF España. Producción total peninsular : Demanda total peninsular : A: . 2016, p. 1-7.

41. Consejo, P.E. y del. Reglamento 1907/2006 del Parlamento Europeo y del Consejo, de 18 de diciembre de 2006, relativo al registro, la evaluación y la restricción de las sustancias y preparados químicos (REACH), por el que se crea la Agencia Europea de Sustancias y Preparados Q. A: *Diario Oficial de la Unión Europea* [en línia]. 2005, p. 1-3. Disponible a: http://echa.europa.eu/es/regulations/reach;jsessionid=12411E70EB80BD2290B756D69F94EEB3.live2.

42. [Online]. CRNE, Centre de Recerca de Nanoenginyeria. A: *UPC-CRNE*. 2016, p. 1.

43. Facultat d'Informàtica de Barcelona. Normativa Prácticas en Empresa UPC. A: *UPB-FIB*. 2015, núm. [Online], p. 14.